J Gastroenterol (2012) 47:1323–1335
DOI 10.1007/s00535-012-0596-x

ORIGINAL ARTICLE—LIVER, PANCREAS, AND BILIARY TRACT

# Sequential immunological analysis of HBV/HCV co-infected patients during Peg-IFN/RBV therapy

**Yasuteru Kondo · Yoshiyuki Ueno · Masashi Ninomiya · Keiichi Tamai · Yasuhito Tanaka · Jun Inoue · Eiji Kakazu · Koju Kobayashi · Osamu Kimura · Masahito Miura · Takeshi Yamamoto · Tomoo Kobayashi · Takehiko Igarashi · Tooru Shimosegawa**

Received: 29 August 2011 / Accepted: 28 March 2012 / Published online: 16 May 2012


## Abstract

*Background* The immunopathogenesis of dual chronic infection with hepatitis B virus and hepatitis C virus (HBV/HCV) remains unclear. The in vivo suppressive effects of each virus on the other have been reported. In this study we aimed to analyze the virological and immunological parameters of HBV/HCV coinfected patients during pegylated interferon/ribavirin (Peg-IFN/RBV) therapy.

*Methods* One patient with high HBV-DNA and high HCV-RNA titers (HBV-high/HCV-high) and 5 patients with low HBV-DNA and high HCV-RNA titers (HBV-low/HCV-high) were enrolled. Twenty patients monoinfected with HBV and 10 patients monoinfected with HCV were enrolled as control subjects.. In vitro cultures of Huh 7 cells with HBV/HCV dual infection were used to analyze the direct interaction of HBV/HCV.

*Results* Direct interaction of HBV clones and HCV could not be detected in the Huh-7 cells. In the HBV-high/HCV-high-patient, the HCV-RNA level gradually declined and HBV-DNA gradually increased during Peg-IFN/RBV therapy. Activated CD4- and CD8-positive T cells were increased at 1 month of Peg-IFN/RBV-therapy, but HBV-specific IFN-$\gamma$-secreting cells were not increased and HBV-specific interleukin (IL)-10 secreting cells were increased. The level of HBV- and HCV-specific IFN-$\gamma$-secreting cells in the HBV-high/HCV-high-patient was low in comparison to that in the HBV- or HCV-monoinfected patients. In the HBV-low/HCV-high-patient, HCV-RNA and HBV-DNA rapidly declined during Peg-IFN/RBV therapy. Activated CD4- and CD8-positive T cells were increased, and HBV- and HCV-specific IFN-$\gamma$-secreting cells were also increased during Peg-IFN/RBV-therapy.

*Conclusion* The immunological responses of the HBV-high/HCV-high patient were low in comparison to the responses in HBV and HCV monoinfected patients. Moreover, the response of immune cells in the HBV-high/HCV-high patient during Peg-IFN/RBV therapy was insufficient to suppress HBV and HCV.

**Keywords** Dual infection · HBV · HCV · Immunopathogenesis

**Electronic supplementary material** The online version of this article (doi:10.1007/s00535-012-0596-x) contains supplementary material, which is available to authorized users.

Y. Kondo · Y. Ueno (✉) · M. Ninomiya · K. Tamai · J. Inoue · E. Kakazu · O. Kimura · T. Shimosegawa
Division of Gastroenterology, Tohoku University Graduate School of Medicine, 1-1 Seiryo, Aobaku, Sendai, Miyagi, Japan
e-mail: y-ueno@med.id.yamagata-u.ac.jp; yeuno@med.tohoku.ac.jp

Y. Tanaka
Virology and Liver Unit, Nagoya City University Medical School, Nagoya, Japan

K. Kobayashi
Tohoku University Graduate School of Medicine, 2-1 Seiryo, Aobaku, Sendai, Miyagi, Japan

M. Miura
Department of Gastroenterology, South Miyagi Medical Center, Oogawara, Miyagi, Japan

T. Yamamoto
Department of Gastroenterology, Tohoku Kosei-Nenkin Hospital, Sendai, Miyagi, Japan

T. Kobayashi
Department of Hepatology, Tohoku Rosai Hospital, Sendai, Miyagi, Japan

T. Igarashi
Department of Gastroenterology, Osaki Citizen Hospital, Osaki, Japan

## Introduction

Hepatitis B virus (HBV) and Hepatitis C virus (HCV) are noncytopathic viruses that cause chronic hepatitis and hepatocellular carcinoma (HCC) [1, 2]. HBV now affects more than 400 million people worldwide, and persistent infection develops in ~5 % of adults and 95 % of neonates who become infected with HBV [3]. HCV infects about 170 million people worldwide and is a major cause of chronic hepatitis, cirrhosis, and HCC [4]. Some groups have mentioned that dual infection with HBV/HCV is not uncommon in Asian patients [5, 6]. The prevalence of patients with dual HBV/HCV infection is approximately 10–15 %, although it likely differs among countries [7–9]. Co-infection with HBV/HCV has been associated with severe liver disease and frequent progression to cirrhosis [10]. Moreover, a significantly higher incidence of HCC and liver-related mortality was noted in patients with HBV/HCV co-infection [11, 12]. However, some groups reported, based on a meta-analysis, that dual infection with HBV/HCV did not increase the risk of HCC [13, 14]. These contradictory reports could be explained by the rarity of dual infection with HBV/HCV in patients without clinically evident liver disease. It might be difficult to estimate the hepatocarcinogenic risk of dual infection compared with that of either infection alone in such clinical settings [15].

An inverse relationship in the replicative levels of the two viruses has been noted, suggesting direct or indirect effects in vivo [16]. More recently, some groups have reported, using an in vitro infection system, that there is little direct interaction of HBV/HCV in coinfected hepatocytes [17, 18]. Therefore, the viral interference observed in coinfected patients is probably due to indirect mechanisms mediated by the innate and/or adaptive host immune responses.

The cellular immune response to HBV and HCV plays an important role in the pathogenesis of chronic hepatitis, cirrhosis, and HCC [19–21]. Hyporesponsiveness of HBV- or HCV-specific T-helper 1 cells and excessive regulatory function of $CD4^+CD25^+FoxP3^+$ regulatory T cells (Tregs) in peripheral blood have been shown in patients with chronic hepatitis B and C [22–34]. Recently, we reported that HBV replication stress could enhance the suppressive activity of Tregs via TLR2 [35]. However, little is known about the immunopathogenesis of HBV/HCV dual infection.

Dual infection can be classified into several groups (e.g., group A: HBV active and HCV active; group B: HBV inactive and HCV active; and group C: HBV active and HCV inactive) [36]. HCV is reported to be the dominant virus in HBV/HCV dual infection, but the dominance of either virus might be due to the genotypes of each virus and/or ethnic differences that could affect the proliferative activity of the viruses [36]. In this study, we investigated immunopathogenesis in a group A patient and in group B patients during therapy with pegylated interferon-α2b (Peg-IFN-α2b) plus ribavirin.

## Patients, materials, and methods

### Patients

One patient with high HBV-DNA and high HCV-RNA titers (HBV-high/HCV-high; patient A) and 5 patients with low HBV-DNA and high HCV-RNA titers (HBV-low/HCV-high) were enrolled (one of these patients, whose results were analyzed in detail, was termed patient B; see findings below in the "Results"). Twenty patients monoinfected with HBV and 10 patients monoinfected with HCV were enrolled as control subjects. None of the patients had liver disease due to other causes, such as alcohol, drugs, congestive heart failure, or autoimmune diseases. Permission for the study was obtained from the Ethics Committee at Tohoku University Graduate School of Medicine (permission no. 2006-194). Written informed consent was obtained from all the participants enrolled in this study. Participants were monitored for two years. At each assessment, patients were evaluated by biochemical laboratory tests, immunological analysis, and virological tests. Liver histology was analyzed at the start of Peg-IFN/RBV therapy by using laparoscopic liver biopsy samples and by employment of the METAVIR score.

### Detection of interleukin (IL)-28B polymorphism

Genomic DNA was isolated from peripheral blood mononuclear cells (PBMCs) using an automated DNA isolation kit. Then polymorphism of IL-28B (rs8099917) was analyzed using real-time polymerase chain reaction (PCR) (TaqMan SNP Genotyping Assay, Applied Biosystems, CA, USA). Detection of the IL-28B polymorphism was approved by the Ethics Committee at Tohoku University Graduate School of Medicine (permission no. 2010-323).

### Isolation of peripheral blood mononuclear cells (PBMCs) and flow cytometry

Peripheral blood mononuclear cells (PBMCs) were isolated from fresh heparinized blood by means of Ficoll-Hypaque density gradient centrifugation (Amersham Bioscience, Uppsala, Sweden). PBMCs were stained with CD3, CD4, CD8, CD19, CD25, CD40, CD56, CD86, HLA-DR, NKG2D, and isotype control antibodies (Becton Dickinson, NJ, USA) for 15 min on ice to analyze the frequency

of $CD3^+CD4^+$HLA-$DR^+$ cells, $CD3^+CD8^+$HLA-$DR^+$cells, $CD4^+CD25^+$ Tregs, $CD3^-CD16^-CD56^{high}$natural killer (NK) cells, and $CD3^-CD16^+CD56^{dim}$ NK cells. The frequencies of the immune subsets were analyzed by flow cytometry using FACS Canto-II (Becton Dickinson, NJ, USA).

### ELISPOT assay

The detection of IFN-$\gamma$ and IL-10 was performed using an ELISPOT Set (BD Biosciences, San Jose, CA, USA) according to the manufacturer's instructions. Cultures of PBMCs were established in triplicate on round-bottomed 96-well plates for all time points investigated, at a concentration of $3 \times 10^5$ cells per well in 100 μl RPMI 1640 containing 10 % fetal bovine serum (FBS). Positive spots were detected using an automated counting machine.

### Detection of HBV-DNA and determination of HBV genotype

DNA was extracted from 100 μl of serum using SMITEST EX-R&D (Medical & Biological Laboratories, Nagoya, Japan) and dissolved in 20 μl of nuclease-free distilled water. The DNA preparation thus obtained (10 μl) was subjected to nested PCR with primers targeting the S gene of the HBV-DNA, as described previously [37]. Briefly, first-round PCR was carried out for 35 cycles (98 °C for 10 s, 55 °C for 15 s, and 72 °C for 1 min, with an additional 7 min in the last cycle) in the presence of PrimeSTAR HS DNA Polymerase (TaKaRa Bio, Shiga, Japan) and primers HB095 (sense, 5′-GAG TCT AGA CTC GTG GTG GAC-3′) and HB184 (antisense, 5′-CGA ACC ACT GAA CAA ATG GCA CCG-3′), for 25 cycles. This was followed by a second-round PCR consisting of 25 cycles using the same conditions as in the first round, with primers HB097 (sense, 5′-GAC TCG TGG TGG ACT TCT CTC-3′) and S2-2 (antisense, 5′-GGC ACT AGT AAA CTG AGC CA-3′). The HBV genotype was determined by phylogenetic analysis of the S gene sequence (437 nt) of the HBV isolates.

### Detection of HCV RNA

RNAs were extracted from 250 μl of serum using TRIzol LS (Invitrogen, Tokyo, Japan). They were divided into two aliquots and each was assayed by reverse transcription (RT)-PCR with nested primers derived from the core region and NS5A interferon sensitivity determining region (ISDR) of the HCV genome. Nested PCR of the core region of the HCV genome was carried out with primers C008 (sense, 5′-AAC CTC AAA GAA AAA CCA AAC G-3′) and C011 (antisense, 5′-CAT GGG GTA CAT YCC GCT YG-3′) in the first round and C009 (sense, 5′-CCA CAG GAC GTY AAG TTC CC-3′) and C010 (antisense, 5′-AGG GTA TCG ATG ACC TTA CC-3′) in the second round. Nested primers that were derived from NS5A-ISDR of the HCV genomes were designed to amplify a 188-bp product with C004 (sense, 5′-ATG CCC ATG CCA GGT TCC AG-3′) and C005 (antisense, 5′-AGC TCC GCC AAG GCA GAA GA-3′) in the first round, and C006 (sense, 5′-ACC GG A TGT GGC AGT GCT CA-3′) and C007 (antisense, 5′-GTA ATC CGG GCG TGC CCA TA-3′) in the second round.

### Analysis of nucleotide and amino acid sequences

The PCR products were sequenced directly on both strands using a BigDye Terminator version 3.1 Cycle Sequencing Kit on an ABI PRISM 3100 Genetic Analyzer (Applied Biosystems, Foster City, CA, USA). Sequence analysis was performed using Genetyx-Mac ver. 12.2.6 (Genetyx, Tokyo, Japan) and ODEN (version 1.1.1) from the DNA Data Bank of Japan (National Institute of Genetics, Mishima, Japan) [38]. Sequence alignments were generated using CLUSTAL W (Version 1.8) [39]. The phylogenetic tree was constructed by the neighbor-joining method [40]. The reliability of the phylogenetic results was assessed using 1000 bootstrap replicants [41]. The final tree was obtained with the Njplot program (version 2.2) [42].

### Plasmid construction

HBV expression plasmids were constructed by previously published methods. Serum samples were obtained from two patients infected with HBV genotype Bj and two patients infected with HBV genotype C. HBV-DNA was extracted from 100 μl serum using a QIAamp DNA blood kit (QIAGEN, Hilden, Germany). Four primer sets were designed to amplify two fragments covering the entire HBV genome. Amplified fragments were inserted into a pGEM-T Easy Vector (Promega, Madison, WI, USA) and cloned in DH5a competent cells (TOYOBO, Osaka, Japan). Briefly, at least 5 clones of each fragment were sequenced and the consensus sequence was identified and used as a template for 1.24-fold the HBV genome of different genotypes (B1 indicates the genotype Bj35 clone; B2 indicates the genotype Bj56 clone; C1 indicates the genotype C-AT clone; and C2 indicates the genotype C-22 clone). The HCV-JFH-1 strain was provided by Dr. T. Wakita (National Institute of Infectious Diseases, Japan).

### HCV and HBV expression in Huh 7 cells

Cell-culture-derived infectious HCV was generated as described previously [43]. The HCV was quantified as

follows: RNA was extracted from the Huh-7 culture supernatant using a QIAamp Viral RNA Kit (Qiagen, Valencia, CA, USA). The HCV RNA was quantified by real-time RT-PCR, using TaqMan EZ RT-PCR Core Reagents (Applied Biosystems) according to the manufacturer's protocol, using the published primers and probe [44]. The filtered (0.45 μm) culture supernatant of HCV-infected Huh-7 cells containing $2 \times 10^8$ HCV RNA copies/ml [equivalent to $9.7 \times 10^4$ focus-forming units (ffu)/ml] was used for the experiments. To analyze HCV-RNA in the supernatant, Huh-7 cells ($2 \times 10^5$ cells in a 6-well plate) were infected with JFH-1 (multiplicity of infection [MOI] = 0.01) and after 4 h the cells were washed twice with phosphate-buffered saline (PBS). The supernatants were then collected and the cells were reseeded at $2 \times 10^5$ cells per 6-well plate. Then the HBV expression and mock plasmid were transfected by FuGENE6 (Roche Applied Science, IN, USA). The supernatant of the culture medium was collected 72 h after transfection. Quantification of HBV-DNA and HCV-RNA was carried out using real-time PCR.

IFN-α was added 24 h after the transfection of the HBV plasmids, and the supernatant of the culture medium was then collected 48 h after the addition of the IFN-α.

## Results

### Clinical characteristics of patients A and B

*Patient A (high HBV-DNA titer and high HCV-RNA titer)*

Patient A was a 44 year-old man with a high aspartate aminotransferase/alanine aminotransferase (AST/ALT) level. The prothrombin time-international normalized ratio (PT-INR) was in the normal range. Patient A had high HBV-DNA titers and high HCV-RNA titers (Table 1). His liver histology was classified as A2/F3 (Fig. 1). The laparoscopic analysis indicated moderate inflammation and intermediate fibrosis. The liver surfaces of the right lobe and left lobe were almost the same phenotype. Polymorphism of IL-28B (rs8099917) was T/G (hetero allele).

*Patient B (low HBV-DNA titer and high HCV-RNA titer)*

Patient B was a 63 year-old man with a low AST/ALT level. PT-INR was in the normal range. Patient B had low HBV-DNA titers and high HCV-RNA titers. The liver histology was classified as A2/F1 (Fig. 1). The liver surface showed moderate inflammation and was smooth. The polymorphism of IL-28B (rs8099917) was T/T (major homo allele).

Biopsy samples from patients with dual HBV and HCV infection were collected at the main liver centers in Miyagi prefecture. Fifteen HBV/HCV dual-infected patients were found in this study (Supplementary Table 1). Many of these patients had HCV-dominant infection and undetectable levels of HBV replication (10/15 patients). Most of the patients were HB envelope antigen (eAg)-negative and HBe antibody (Ab)-positive (14/14 patients). All HBV/HCV dual-infected patients who had received Peg-IFN-based

**Table 1** Background of HBV/HCV dual-infected patients

| | Patient A HCV high titer/ HBV high titer | Patient B HCV high titer/ HBV low titer | Normal range |
|---|---|---|---|
| Gender | Male | Male | |
| Age (years) | 44 | 63 | |
| HCV-RNA | 6.5 | 5.5 | log copies/ml |
| HCV genotype | 1b | 1b | |
| HBV-DNA | 5.5 | 3.5 | log copies/ml |
| HBV genotype | C | Bj | |
| HBe-Ag | 129.5 | 0.5 | 0–0.9 index |
| HBe-Ab | 0.1 | 99.3 | 0–49 % |
| Total bilirubin | 0.7 | 1.2 | 0.2–1.2 mg/dl |
| Direct bilirubin | 0.1 | 0.1 | 0–0.3 mg/dl |
| γ-GTP | 208 | 31 | 8–57 IU/l |
| AST | 138 | 33 | 12–30 IU/l |
| ALT | 256 | 38 | 8–35 IU/l |
| Hb-A1c | 5.3 | 5.4 | 4.3–5.8 % |
| Glu | 103 | 83 | 68–106 mg/dl |
| BMI | 25.34 | 18.75 | |
| T-cho | 160 | 195 | 128–220 mg/dl |
| LDL-cho | 69 | 93 | 70–139 mg/dl |
| HDL-cho | 37 | 67 | 36–89 md/dl |
| WBC | 7800 | 5100 | 3200–9600/μl |
| RBC | 491 | 446 | 428–566 × $10^4$/μl |
| Hb | 17.1 | 14.1 | 13.6–17.4 g/dl |
| PLT | 169000 | 176000 | 155000–347000/μl |
| PT-INR | 0.87 | 0.96 | 0–1.15 INR |
| Liver histology | A2/F3 | A2/F1 | METAVIR score |
| IL-28B SNP (rs8099917) | T/G | T/T | |

*HCV* hepatitis C virus, *HBV* hepatitis B virus, e-*Ag* envelope antigen, *e-Ab* envelope antibody, *γ-GTP* γ-guanosine triphosphate, *AST* aspartate aminotransferase, *ALT* alanine aminotransferase, *Hb* hemoglobin, *Glu* glucose, *BMI* body mass index, *T-cho* total cholesterol, *LDL* low-density lipoprotein, *HDL* high-density lipoprotein, *PLT* platelets, *PT-INR* prothromin time-international normalized ratio, *IL* interleukin, *SNP* single-nucleotide polymorphism

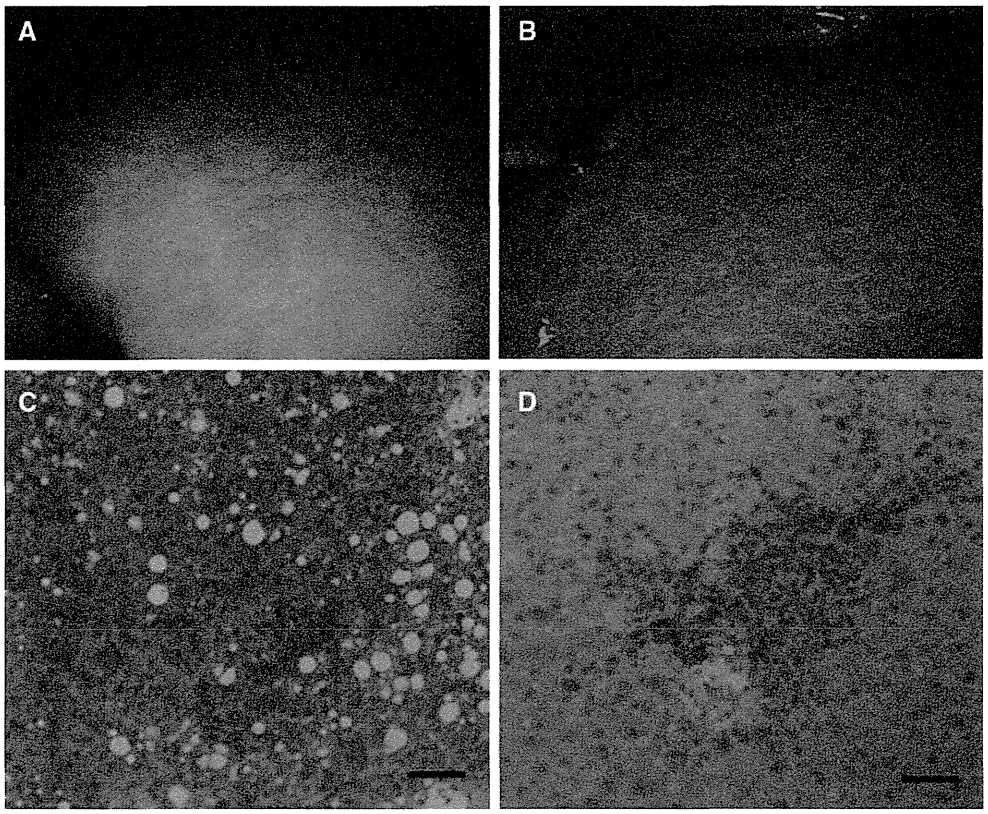


**Fig. 1** Laparoscopic liver biopsy. The laparoscopic images of the liver surfaces of patient A (**a**) and patient B (**b**) are shown. Histopathology of patient A (**c**) and patient B (**d**) is also shown. *Bars* = 50 μm

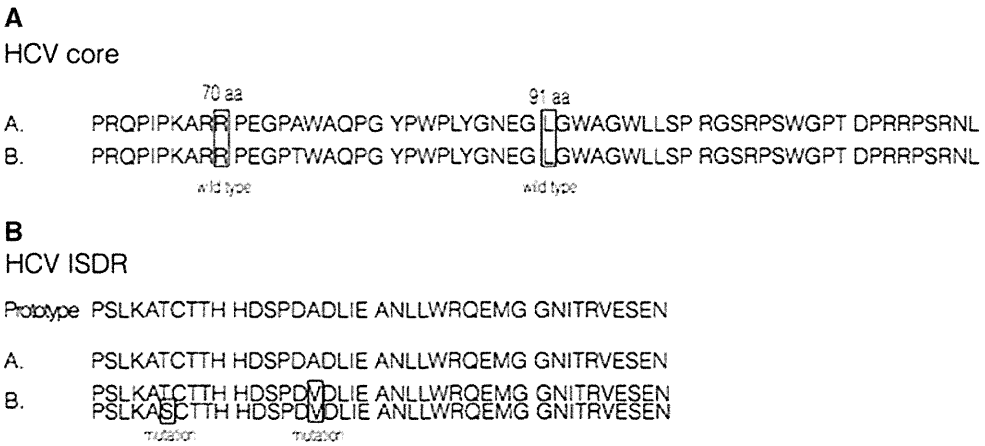


**Fig. 2** Virological analysis of hepatitis B virus (HBV) and hepatitis C virus (HCV) in HBV/HCV dual infection. The amino acid sequences of the HCV-core region including core-70 and core-91, which were previously reported as determinants of the sensitivity to pegylated interferon/ribavirin (Peg-IFN/RBV) therapy, in patient A and patient B are shown (**a**). The amino acid sequences of the interferon sensitivity determining region (*ISDR*), which were previously reported as determinants of the sensitivity to IFN, in patients A and B are shown (**b**)

treatment achieved a sustained viral response (SVR) (5/5 patients). These data indicated that HCV-dominant dual-infected patients had good responses to treatment for HCV infection.

Virological analysis of HBV/HCV in patients A and B

The HCV genotype in both patient A and patient B was 1b. The sequences of amino acids in the ISDR region and HCV

core-70 and core-91 amino acids were analyzed by direct sequencing. Both patients had wild-type core-70 and core-91 amino acids (Fig. 2a). None of the mutations of the ISDR region was detected in patient A, but two of the mutations of the ISDR region were detected in patient B (Fig. 2b). The genotypes of HBV in patients A and B were analyzed by direct sequencing and phylogenetic tree analysis. The genotype of HBV in patient A was genotype C, which has been reported as difficult-to-treat HBV. The genotype of HBV in patient B was genotype Bj, which has been reported as easy-to-treat HBV in comparison to genotype C [45–47].

## Sequential analysis of biochemical and virological data during Peg-IFN/RBV therapy

### *Patient A*

In patient A, HCV-RNA gradually declined during Peg-IFN/RBV therapy. On the other hand, the HBV-DNA gradually increased during Peg-IFN/RBV therapy (Fig. 3a). The amount of HBeAg started to increase 9 months after the start of Peg-IFN/RBV therapy. HCV-RNA started to increase 12 months after the start of Peg-IFN/RBV therapy, although Peg-IFN/RBV was still being administered up to 18 months after the start of Peg-IFN/RBV therapy (Fig. 3a).

### *Patient B*

In patient B, HCV-RNA and HBV-DNA rapidly declined after the start of Peg-IFN/RBV therapy (Fig. 3b). HCV-RNA could not be detected in peripheral blood 2 months after the start of Peg-IFN/RBV therapy. Peg-IFN/RBV was administered up to 12 months after the start of the Peg-IFN/RBV therapy. The amounts of HBeAb and HBeAg did not change during the Peg-IFN/RBV therapy (Fig. 3b).

## Sequential immunological analysis during Peg-IFN/RBV therapy

We analyzed various subsets of immune cells that could affect the immunopathogenesis of HBV/HCV dual infection. NK cells ($CD3^-CD16^-CD56^{high}$ and $CD3^-CD16^+CD56^{dim}$) and NK-T cells ($CD3^+CD56^+CD16^+$, $CD3^+CD56^+CD16^-$ and $CD3^+CD56^-CD16^+$) were analyzed (Supplementary Fig. 1A). The $CD3^-$ gated lymphocytes were separated into 4 groups (a, b, c, and d). For these subsets, (a) indicated the presence of $CD3^-CD16^-CD56^{high}$ NK cells that could produce various cytokines vigorously and had low cytotoxic activity. Subset (b) showed $CD3^-CD16^+CD56^{dim}$ NK cells that had weak cytokine production ability and high cytotoxic activity.

The $CD3^+$ gated lymphocytes were separated into 3 groups (a, b, and c). The activated $CD3^+$, $CD3^+CD4^+$, and $CD3^+CD8^+$ T cells were analyzed (Supplementary Fig. 1B). HLA-$DR^+$ activated $CD3^+$, $CD3^+CD4^+$, and $CD3^+CD8^+$ T cells could be clearly distinguished by FACS analysis. Additionally, representative dot plots of Tregs and B cells were created (shown in Supplementary Fig. 1C). The frequencies of $CD3^-CD16^+CD56^{dim}$ NK cells, $CD3^+CD16^-CD56^+$ NK-T cells, activated $CD3^+CD4^+$ T cells, and activated $CD3^+CD8^+$ T cells fluctuated similarly during Peg-IFN/RBV therapy in patient A (Supplementary Fig. 1D). Activated T cells were increased at one month of Peg-IFN/RBV therapy, and the above subsets of lymphocytes gradually decreased up to 3 months of Peg-IFN/RBV therapy. After that, these cells gradually increased again up to 9 months of Peg-IFN/RBV therapy. In patient A, after 9 months of Peg-IFN/RBV therapy, these cells had decreased again (Supplementary Fig. 1D). The frequency of Tregs and activated B cells (data not shown) did not change during Peg-IFN/RBV therapy in patient A (Supplementary Fig. 1D). On the other hand, in patient B, the frequencies of $CD3^-CD16^+CD56^{dim}$ NK cells, $CD3^+CD16^-CD56^+$ NK-T cells, activated $CD3^+CD4^+$ T cells, and activated $CD3^+CD8^+$ T cells were increased and sustained during Peg-IFN/RBV therapy (Supplementary Fig. 1E). Five HCV monoinfected patients were analyzed by the same protocol (Supplementary Fig 1F). The mean frequency of various kinds of immune subsets was analyzed (Supplementary Fig 1F). The tendency of immunological reactions during Peg-IFN/RBV therapy in these five patients was similar to that in patient B.

## Analysis of HBV- and HCV-specific immune responses

The analysis of HBV- and HCV-specific-immune responses was carried out by ELISPOT assay. Representative spots of IFN-$\gamma$ are shown in Fig. 4a. In patient A, HCV- and HBV-specific IFN-$\gamma$ secretion activities were remarkably low in comparison to the IL-10 secretion activity. Moreover, in patient A, the induction of IFN-$\gamma$-secreting cells could not be detected after Peg-IFN/RBV therapy, especially in regard to HBV-core specific IFN-$\gamma$ secretion in PBMCs (Fig. 4b). On the other hand, in patient B, the HBV-core specific IFN-$\gamma$-secreting cells were high in comparison to those in patient A (Fig. 4c). Moreover, the induction of IFN-$\gamma$-secreting cells could be detected during Peg-IFN/RBV therapy in patient B (Fig. 4c). The mean numbers of IFN-$\gamma$- and IL-10-secreting spots in HBV-dominant dual-infected patients, patients with monoinfection with HBV genotype Bj ($HBeAb^+$), Bj ($HBeAg^+$), C ($HBeAb^+$), C ($HBeAg^+$), or HCV genotype 1b are shown in Fig. 4d. In patient A, HB core antigen (HBcAg)-specific IFN-$\gamma$ secretion was weaker than that in

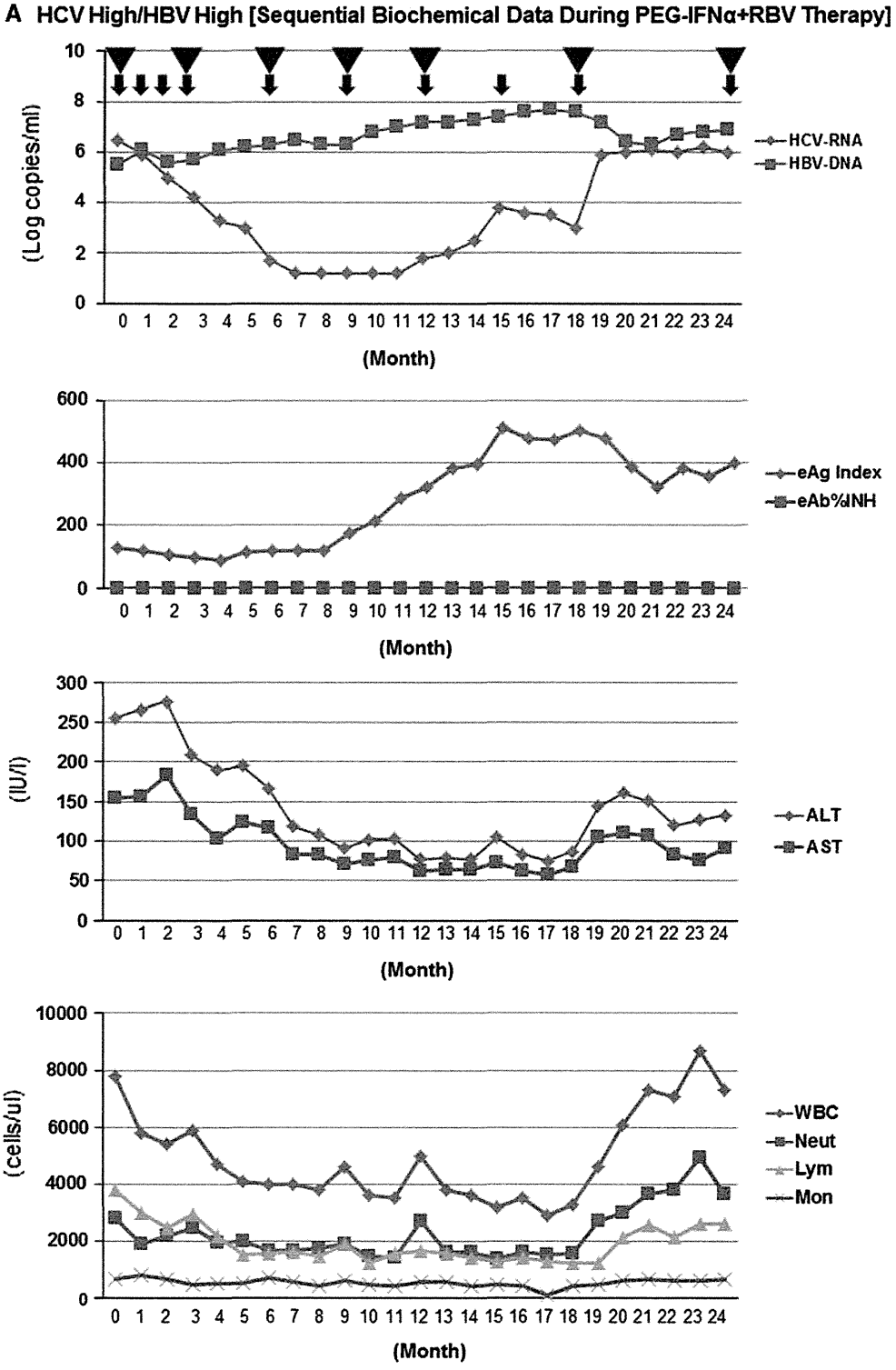


**Fig. 3** Sequential biochemical data analysis during Peg-IFN/RBV therapy. The titers of HBV-DNA and HCV-RNA; the amounts of envelope antigen (*eAg*) and envelope antibody (*eAb*), and alanine aminotransferase (*ALT*) and aspartate aminotransferase (*AST*); and the numbers of WBCs, neutrophils (*Neut*), lymphocytes (*Lym*), and monocytes (*Mon*) in patients A (**a**) and B (**b**) are shown in these graphs. *Arrows* indicate the sampling points of FACS analysis. *Triangles* indicate the sampling points of the ELISPOT assay. *INH* inhibition

HBV-genotype C-monoinfected patients who were HBeAg-positive. However, HBcAg-specific IL-10 secretion in patient A was stronger than that in HBV-genotype C monoinfected patients who were HBeAg-positive. These data indicated that the presence of HCV might also suppress the HBV-specific immune response in regard to certain host factors (e.g., in the presence of IL-28B polymorphism, and depending on the body mass index [BMI] and γ-guanosine triphosphate [γ-GTP] level), because the presence of HCV did not suppress the HBV-specific immune response either in patient B or in the patients with dual HCV-dominant infection. Otherwise, we could deny the possibility indicating that

Fig. 3 continued

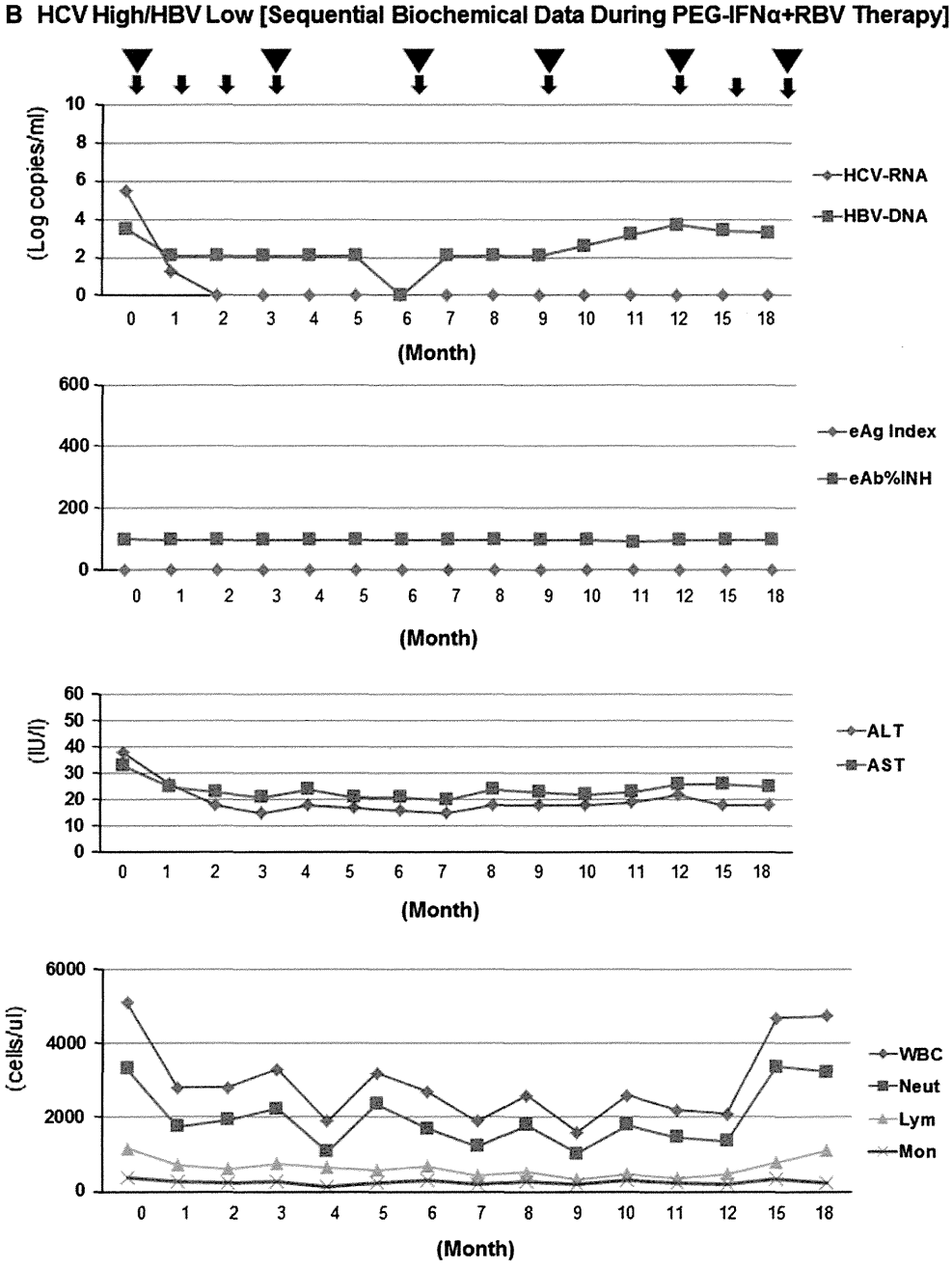


the certain background of host factors could allow the existence of dual virus actively. These data indicated that HBV-specific IL-10-secreting cells and/or certain kinds of host factors had an important role in HBV- and HCV-specific immune suppression in patient A, but not in patient B.

In vitro analysis of HBV/HCV dual infection

We carried out in vitro analysis of HBV/HCV infection using Huh-7 cells that were susceptible to the HCV-JFH-1 strain and HBV expression plasmids. The amount of the JFH-1 strain did not change with the various kinds of HBV expression plasmids (Fig. 5a). Moreover, the amounts of the various HBV strains did not change in the presence of JFH-1 infection. These data indicated that no direct effect of HBV and HCV could be detected in Huh 7 cells. We carried out experiments to analyze the effect of IFN-α treatment on HCV Huh-7 cells with various kinds of HBV expression (Fig. 5b). In our systems, it appeared that HBV expression could not significantly affect the suppressive effect of IFN-α.

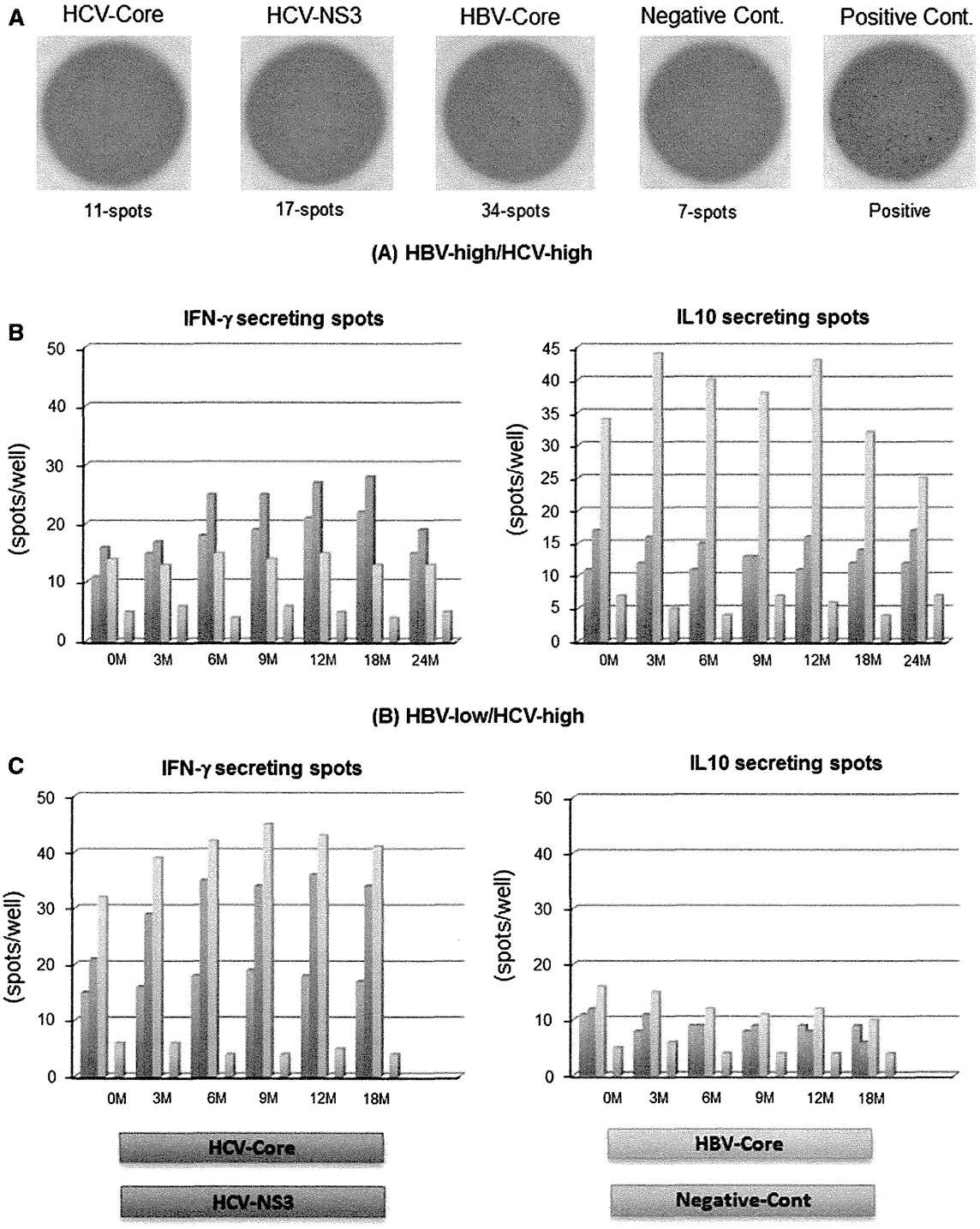


**Fig. 4** The sequential analysis of HBV/HCV-specific immune reactions during Peg-IFN/RBV therapy. Representative spots of the ELISPOT assay are shown (**a**). The sequential data of IFN-$\gamma$- and interleukin-10 (*IL-10*)- secreting spots in patient A are shown (**b**). The sequential data of IFN-$\gamma$- and IL-10-secreting spots in patient B are shown (**c**). Comparison of IFN-$\gamma$- and IL-10- secreting spots in patient A before starting therapy, patient B before starting therapy, dual HCV-dominant patients, HCV-monoinfected patients, HBV-Bj ($HBeAb^+$) monoinfected patients, HBV-Bj ($HBeAg^+$) monoinfected patients, HBV-C ($HBeAb^+$) monoinfected patients, and HBV-C ($HBeAg^+$) monoinfected patients (**d**). In these *bar graphs*, the *blue bars* indicate HCV-core specific reaction. The *red bars* indicate HCV-NS3 specific reaction. The *green bars* indicate HBV-core specific reaction. The *aqua blue bars* indicate the negative control (*Cont.*). *Error bars* indicate standard deviations (color figure online)

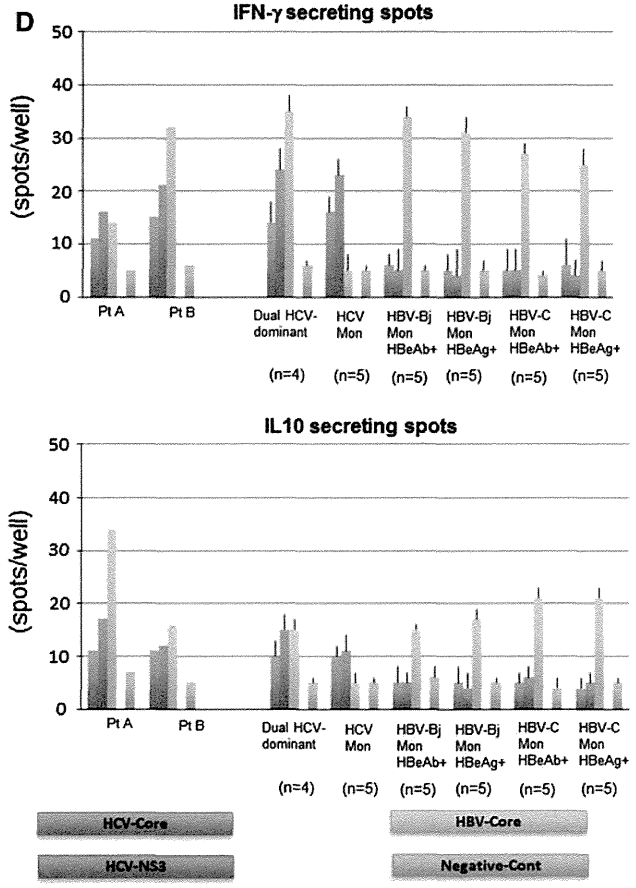


**Fig. 4** continued

## Discussion

The immunopathogenesis of dual hepatitis B and C infection is not clear, given the complexity of viral and host factors [19, 21, 48–50]. However, detailed understanding of specific patients with dual hepatitis B and C infection could contribute to improving the treatment and follow up of these patients. Therefore, we focused on two representative patients with HBV/HCV dual infection who received Peg-IFN/RBV therapy.

Concerning the virological results, patient A had genotype 1b, HCV-Core 70 wild-type and low mutation of ISDR HCV and genotype C HBV. It has been reported that genotype 1b HCV is common in Japan and is usually difficult to treat in comparison to genotypes 2a and 2b [51]. Among genotype 1b HCV strains, HCV-Core 70 wild-type HCV is easily decreased by Peg-IFN/RBV therapy [51]. On the other hand, it has been reported that in genotype 1b HCV low mutation of ISDR is difficult to treat [52]. Patient B had almost the same background of HCV–genotype 1b, HCV-Core 70 wild-type, and low mutation of ISDR–as patient A. However, the background of host factors that could affect the responsiveness of IFN-based therapy was different between patients A and B. For example, patient A had a hetero allele of the IL-28B polymorphism, advanced fibrosis, and fatty changes of the liver. On the other hand, patient B had the major allele of the IL-28B polymorphism and mild fibrosis. Moreover, the background of HBV in patient B was completely different from that in patient A. It has been reported that HBV genotype Bj is usually more susceptible to IFN-based therapy than genotype C [45, 53]. Therefore, not only the HBV factors but also the combination of host factors and HBV factors might affect the responsiveness to IFN-based therapy. In patient A, the responsiveness of HCV during Peg-IFN/RBV therapy was relatively poor. However, the viral titers of HCV were lower than 1.2 log copies/ml at 7 months after the start of therapy. During the reduction of the HCV viral titers, the titers of HBV and HBc-Ag specific IL-10-secreting cells were gradually increased. Although patient A had received Peg-IFN/RBV therapy for up to 18 months, HCV-RNA increased again 12 months after the start of the therapy. The sustained Th1 immune suppression might have contributed to the relapse of HCV. Not only weak up-regulation of HCV-specific Th1 immune reaction but also strong up-regulation of HBV-specific IL-10-secreting activity was detected during Peg-IFN/RBV therapy in patient A [26, 35]. Moreover, increased HBeAg could be detected 9 months after the start of the therapy. Fluctuations of activated CD4 cells, CD8 cells, NK cells, and NK-T cells could be seen in patient A. On the other hand, in patient B, the responsiveness of HBV and HCV during Peg-IFN/RBV therapy was good. Moreover, the immune response of patient B was almost comparable to the responses in the patients with HCV monoinfection and those with HBV-genotype Bj monoinfection. Previously, it has been reported that Peg-IFN/RBV therapy could achieve almost the same SVR rates in patients with HCV/HBV dual infection and those with HCV monoinfection [54–56]. We assume that the results in these studies were obtained from patients similar to our patient B, because the number of patients with HCV-dominant infection is much higher than the number of those with HBV/HCV dual active infection such as our patient A. Patients with HBV/HCV dual active infection such as patient A are relatively rare in Japan. However, it is necessary to understand the immunopathogenesis of these patients, because Peg-IFN/RBV therapy might not be sufficient to eradicate or control HBV/HCV in these difficult-to-treat patients. One of the candidate therapies for such patients might be Entecavir (ETV)/Peg-IFN/RBV sequential therapy. The effect of HBV specific regulatory T cells might contribute to the immunosuppression of not only HBV but also HCV [35]. In some previous studies, including ours, it has been reported that HBV replication might contribute to immune suppression [19, 29].

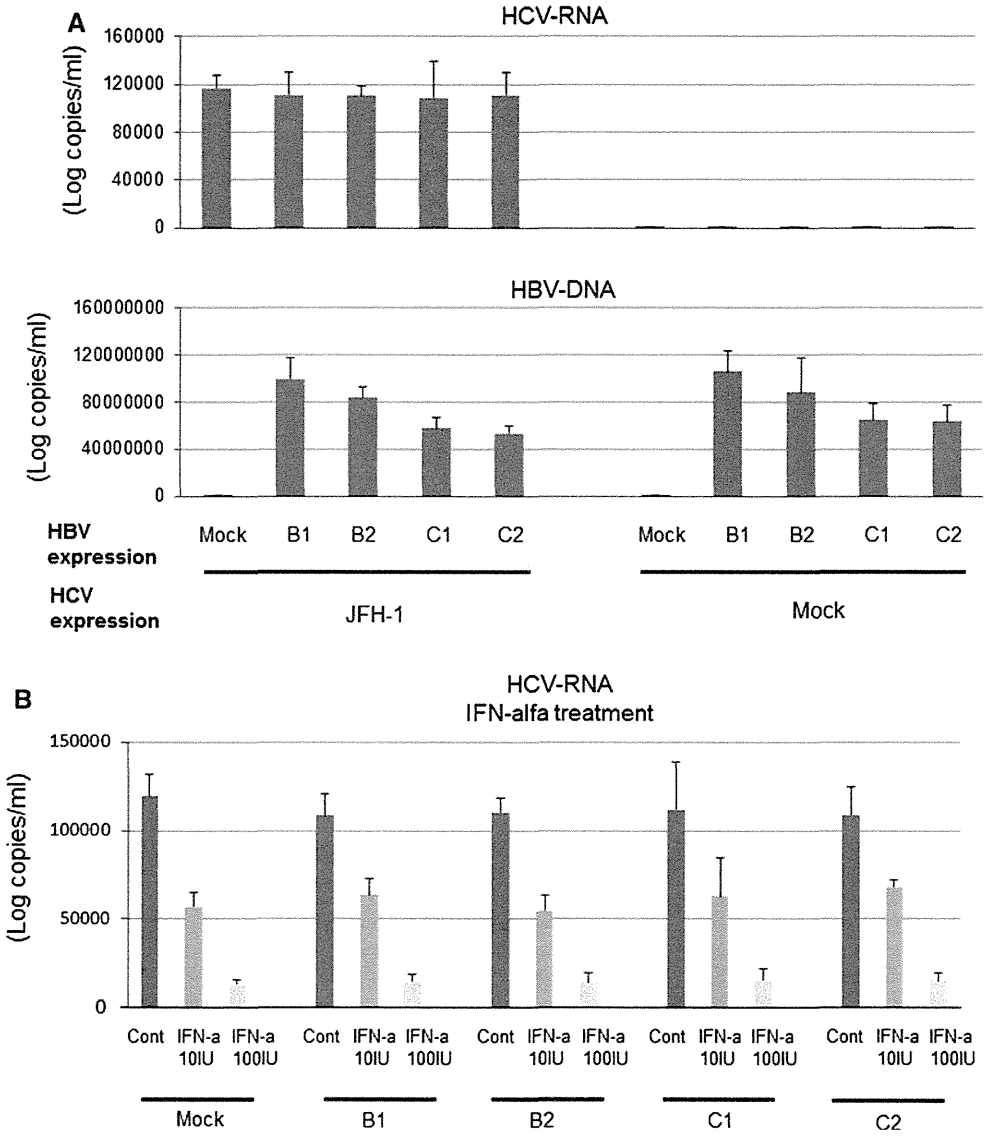


**Fig. 5** In vitro analysis of HBV/HCV dual infection. The titers of HCV-RNA and HBV-DNA are shown. *B1* indicates genotype Bj35 clone. *B2* indicates genotype Bj56 clone. *C1* indicates genotype C-AT clone. *C2* indicates genotype C-22 clone (**a**). The titers of HCV-RNA after the IFN-α treatment are shown (**b**)

In the present study, we employed an in vitro coinfection system to analyze the direct interaction between HBV and HCV. In our system, we used several different HBV clones, because it is necessary to consider the effects of different genotypes. Although we could not detect the direct interaction of HBV/HCV in our system, we could not exclude the possibility of indirect interaction between cytokines and chemokines produced from virus-infected hepatocytes. We are now analyzing the chemokines produced from hepatoma cells with different HBV genotype clones (ongoing study).

In conclusion, we analyzed data from representative patients with HBV/HCV dual infection sequentially and precisely. Because many different kinds of backgrounds might affect immunoreactions, we focused on representative patients and analyzed the immunological responses extensively. There might be a group of patients with very difficult-to-treat dual infections. We need to understand the immunopathogenesis of such patients to develop the appropriate therapy.

**Acknowledgments** This work was supported in part by a Grant-in Aid from the Ministry of Education, Culture, Sport, Science, and Technology of Japan (Y.K. #23790761), and grants from the Ministry of Health, Labor, and Welfare of Japan.

**Conflict of interest** The authors declare that they have no conflict of interest.

## References

1. Alter MJ, Kruszon-Moran D, Nainan OV, et al. The prevalence of hepatitis C virus infection in the United States, 1988 through 1994. N Engl J Med. 1999;341(8):556–62.

2. Tiollais P, Pourcel C, Dejean A. The hepatitis B virus. Nature. 1985;317(6037):489–95.
3. Lai CL, Ratziu V, Yuen MF, Poynard T. Viral hepatitis B. Lancet. 2003;362(9401):2089–94.
4. Poynard T, Yuen MF, Ratziu V, Lai CL. Viral hepatitis C. Lancet. 2003;362(9401):2095–100.
5. Potthoff A, Manns MP, Wedemeyer H. Treatment of HBV/HCV coinfection. Expert Opin Pharmacother. 2010;11(6):919–28.
6. Chu CJ, Lee SD. Hepatitis B virus/hepatitis C virus coinfection: epidemiology, clinical features, viral interactions and treatment. J Gastroenterol Hepatol. 2008;23(4):512–20.
7. Bini EJ, Perumalswami PV. Hepatitis B virus infection among American patients with chronic hepatitis C virus infection: prevalence, racial/ethnic differences, and viral interactions. Hepatology. 2010;51(3):759–66.
8. Halima SB, Bahri O, Maamouri N, et al. Serological and molecular expression of hepatitis B infection in patients with chronic hepatitis C from Tunisia, North Africa. Virol J. 2010;7:229.
9. Saravanan S, Velu V, Nandakumar S, et al. Hepatitis B virus and hepatitis C virus dual infection among patients with chronic liver disease. J Microbiol Immunol Infect. 2009;42(2):122–8.
10. Lee LP, Dai CY, Chuang WL, et al. Comparison of liver histopathology between chronic hepatitis C patients and chronic hepatitis B and C-coinfected patients. J Gastroenterol Hepatol. 2007;22(4):515–7.
11. Liu Z, Hou J. Hepatitis B virus (HBV) and hepatitis C virus (HCV) dual infection. Int J Med Sci. 2006;3(2):57–62.
12. Tsai JF, Jeng JE, Ho MS, et al. Effect of hepatitis C and B virus infection on risk of hepatocellular carcinoma: a prospective study. Br J Cancer. 1997;76(7):968–74.
13. Cho LY, Yang JJ, Ko KP, et al. Coinfection of hepatitis B and C viruses and risk of hepatocellular carcinoma: systematic review and meta-analysis. Int J Cancer. 2011;128(1):176–84.
14. Huo TI, Huang YH, Hsia CY, et al. Characteristics and outcome of patients with dual hepatitis B and C-associated hepatocellular carcinoma: are they different from patients with single virus infection? Liver Int. 2009;29(5):767–73.
15. Kew MC. Interaction between hepatitis B and C viruses in hepatocellular carcinogenesis. J Viral Hepat. 2006;13(3):145–9.
16. Liu CJ, Chen PJ, Chen DS. Dual chronic hepatitis B virus and hepatitis C virus infection. Hepatol Int. 2009;3(4):517–25.
17. Bellecave P, Gouttenoire J, Gajer M, et al. Hepatitis B and C virus coinfection: a novel model system reveals the absence of direct viral interference. Hepatology. 2009;50(1):46–55.
18. Eyre NS, Phillips RJ, Bowden S, et al. Hepatitis B virus and hepatitis C virus interaction in Huh-7 cells. J Hepatol. 2009;51(3):446–57.
19. Chisari FV, Ferrari C. Hepatitis B virus immunopathogenesis. Annu Rev Immunol. 1995;13:29–60.
20. Koziel MJ. The role of immune responses in the pathogenesis of hepatitis C virus infection. J Viral Hepat. 1997;4(Suppl 2):31–41.
21. Rice CM, Walker CM. Hepatitis C virus-specific T lymphocyte responses. Curr Opin Immunol. 1995;7(4):532–8.
22. Nan XP, Zhang Y, Yu HT, et al. Circulating $CD4^{+}CD25^{high}$ regulatory T cells and expression of PD-1 and BTLA on $CD4^{+}$ T cells in patients with chronic hepatitis B virus infection. Viral Immunol. 2010;23(1):63–70.
23. Kondo Y, Ueno Y, Shimosegawa T. Immunopathogenesis of hepatitis B persistent infection: implications for immunotherapeutic strategies. Clin J Gastroenterol. 2009;2(2):71–9.
24. Peng G, Li S, Wu W, Sun Z, Chen Y, Chen Z. Circulating $CD4^{+}$ $CD25^{+}$ regulatory T cells correlate with chronic hepatitis B infection. Immunology. 2008;123(1):57–65.
25. Maier H, Isogawa M, Freeman GJ, Chisari FV. PD-1:PD-L1 interactions contribute to the functional suppression of virus-specific $CD8^{+}$ T lymphocytes in the liver. J Immunol. 2007;178(5):2714–20.
26. Kondo Y, Kobayashi K, Ueno Y, et al. Mechanism of T cell hyporesponsiveness to HBcAg is associated with regulatory T cells in chronic hepatitis B. World J Gastroenterol. 2006;12(27):4310–7.
27. Stoop JN, van der Molen RG, Baan CC, et al. Regulatory T cells contribute to the impaired immune response in patients with chronic hepatitis B virus infection. Hepatology. 2005;41(4):771–8.
28. Kondo Y, Kobayashi K, Asabe S, et al. Vigorous response of cytotoxic T lymphocytes associated with systemic activation of CD8 T lymphocytes in fulminant hepatitis B. Liver Int. 2004;24(6):561–7.
29. Kondo Y, Asabe S, Kobayashi K, et al. Recovery of functional cytotoxic T lymphocytes during lamivudine therapy by acquiring multi-specificity. J Med Virol. 2004;74(3):425–33.
30. Kondo Y, Ueno Y, Kakazu E, et al. Lymphotropic HCV strain can infect human primary naive CD4(+) cells and affect their proliferation and IFN-gamma secretion activity. J Gastroenterol. 2011;46:232–41.
31. Kondo Y, Machida K, Liu HM, et al. Hepatitis C virus infection of T cells inhibits proliferation and enhances fas-mediated apoptosis by down-regulating the expression of CD44 splicing variant 6. J Infect Dis. 2009;199(5):726–36.
32. Kondo Y, Sung VM, Machida K, Liu M, Lai MM. Hepatitis C virus infects T cells and affects interferon-gamma signaling in T cell lines. Virology. 2007;361(1):161–73.
33. Ulsenheimer A, Gerlach JT, Gruener NH, et al. Detection of functionally altered hepatitis C virus-specific CD4 T cells in acute and chronic hepatitis C. Hepatology. 2003;37(5):1189–98.
34. Cramp ME, Rossol S, Chokshi S, Carucci P, Williams R, Naoumov NV. Hepatitis C virus-specific T-cell reactivity during interferon and ribavirin treatment in chronic hepatitis C. Gastroenterology. 2000;118(2):346–55.
35. Kondo Y, Ueno Y, Kobayashi K, et al. Hepatitis B virus replication could enhance regulatory T cell activity by producing soluble heat shock protein 60 from hepatocytes. J Infect Dis. 2010;202(2):202–13.
36. Nguyen LH, Ko S, Wong SS, et al. Ethnic differences in viral dominance patterns in patients with hepatitis B virus and hepatitis C virus dual infection. Hepatology. 2011;53(6):1839–45.
37. Takahashi M, Nishizawa T, Gotanda Y, et al. High prevalence of antibodies to hepatitis A and E viruses and viremia of hepatitis B, C, and D viruses among apparently healthy populations in Mongolia. Clin Diagn Lab Immunol. 2004;11(2):392–8.
38. Ina Y. ODEN: a program package for molecular evolutionary analysis and database search of DNA and amino acid sequences. Comput Appl Biosci. 1994;10(1):11–2.
39. Thompson JD, Higgins DG, Gibson TJ. CLUSTAL W: improving the sensitivity of progressive multiple sequence alignment through sequence weighting, position-specific gap penalties and weight matrix choice. Nucleic Acids Res. 1994;22(22):4673–80.
40. Saitou N, Nei M. The neighbor-joining method: a new method for reconstructing phylogenetic trees. Mol Biol Evol. 1987;4(4):406–25.
41. Felsenstein J. Estimating effective population size from samples of sequences: a bootstrap Monte Carlo integration method. Genet Res. 1992;60(3):209–20.
42. Perriere G, Gouy M. WWW-query: an on-line retrieval system for biological sequence banks. Biochimie. 1996;78(5):364–9.
43. Wakita T, Pietschmann T, Kato T, et al. Production of infectious hepatitis C virus in tissue culture from a cloned viral genome. Nat Med. 2005;11(7):791–6.
44. Takeuchi T, Katsume A, Tanaka T, et al. Real-time detection system for quantification of hepatitis C virus genome. Gastroenterology. 1999;116(3):636–42.

45. Sugauchi F, Kumada H, Sakugawa H, et al. Two subtypes of genotype B (Ba and Bj) of hepatitis B virus in Japan. Clin Infect Dis. 2004;38(9):1222–8.
46. Sugauchi F, Orito E, Ichida T, et al. Epidemiologic and virologic characteristics of hepatitis B virus genotype B having the recombination with genotype C. Gastroenterology. 2003; 124(4):925–32.
47. Orito E, Mizokami M, Sakugawa H, et al. A case–control study for clinical and molecular biological differences between hepatitis B viruses of genotypes B and C. Japan HBV Genotype Research Group. Hepatology. 2001;33(1):218–23.
48. Raimondo G, Brunetto MR, Pontisso P, et al. Longitudinal evaluation reveals a complex spectrum of virological profiles in hepatitis B virus/hepatitis C virus-coinfected patients. Hepatology. 2006;43(1):100–7.
49. Chuang WL, Dai CY, Chang WY, et al. Viral interaction and responses in chronic hepatitis C and B coinfected patients with interferon-alpha plus ribavirin combination therapy. Antivir Ther. 2005;10(1):125–33.
50. Tsai SL, Liaw YF, Yeh CT, Chu CM, Kuo GC. Cellular immune responses in patients with dual infection of hepatitis B and C viruses: dominant role of hepatitis C virus. Hepatology. 1995;21(4):908–12.
51. Akuta N, Suzuki F, Hirakawa M, et al. Amino acid substitution in hepatitis C virus core region and genetic variation near the interleukin 28B gene predict viral response to telaprevir with peginterferon and ribavirin. Hepatology. 2010;52(2):421–9.
52. Fukuma T, Enomoto N, Marumo F, Sato C. Mutations in the interferon-sensitivity determining region of hepatitis C virus and transcriptional activity of the nonstructural region 5A protein. Hepatology. 1998;28(4):1147–53.
53. Akuta N, Kumada H. Influence of hepatitis B virus genotypes on the response to antiviral therapies. J Antimicrob Chemother. 2005;55(2):139–42.
54. Yu ML, Lee CM, Chuang WL, et al. HBsAg profiles in patients receiving peginterferon alfa-2a plus ribavirin for the treatment of dual chronic infection with hepatitis B and C viruses. J Infect Dis. 2010;202(1):86–92.
55. Yu JW, Sun LJ, Zhao YH, Kang P, Gao J, Li SC. Analysis of the efficacy of treatment with peginterferon alpha-2a and ribavirin in patients coinfected with hepatitis B virus and hepatitis C virus. Liver Int. 2009;29(10):1485–93.
56. Liu CJ, Chuang WL, Lee CM, et al. Peginterferon alfa-2a plus ribavirin for the treatment of dual chronic infection with hepatitis B and C viruses. Gastroenterology. 2009;136((2)):496.e3–504.e3.

# FGF7 is a functional niche signal required for stimulation of adult liver progenitor cells that support liver regeneration

Hinako M. Takase,[1,5,6] Tohru Itoh,[1,5,7] Seitaro Ino,[1] Ting Wang,[2] Takehiko Koji,[3] Shizuo Akira,[4] Yasuhiro Takikawa,[2] and Atsushi Miyajima[1]

[1]Laboratory of Cell Growth and Differentiation, Institute of Molecular and Cellular Biosciences, The University of Tokyo, Tokyo 113-0032, Japan; [2]Division of Gastroenterology and Hepatology, Department of Internal Medicine, Iwate Medical University, Iwate 020-8505, Japan; [3]Department of Histology and Cell Biology, Nagasaki University Graduate School of Biomedical Sciences, Nagasaki 852-8523, Japan; [4]Laboratory of Host Defense, World Premier International Immunology Frontier Research Center, Osaka University, Osaka 565-0871, Japan

**The liver is a unique organ with a remarkably high potential to regenerate upon injuries. In severely damaged livers where hepatocyte proliferation is impaired, facultative liver progenitor cells (LPCs) proliferate and are assumed to contribute to regeneration. An expansion of LPCs is often observed in patients with various types of liver diseases. However, the underlying mechanism of LPC activation still remains largely unknown. Here we show that a member of the fibroblast growth factor (FGF) family, FGF7, is a critical regulator of LPCs. Its expression was induced concomitantly with LPC response in the liver of mouse models as well as in the serum of patients with acute liver failure. *Fgf7*-deficient mice exhibited markedly depressed LPC expansion and higher mortality upon toxin-induced hepatic injury. Transgenic expression of FGF7 in vivo led to the induction of cells with characteristics of LPCs and ameliorated hepatic dysfunction. We revealed that Thy1$^+$ mesenchymal cells produced FGF7 and appeared in close proximity to LPCs, implicating a role for those cells as the functional LPC niche in the regenerating liver. These findings provide new insights into the cellular and molecular basis for LPC regulation and identify FGF7 as a potential therapeutic target for liver diseases.**

[*Keywords*: liver regeneration; progenitor cells; niche signal; FGF7; Thy1$^+$ cells]

Supplemental material is available for this article.

Received August 31, 2012; revised version accepted December 13, 2012.

In the liver, hepatocytes and cholangiocytes (bile duct epithelial cells [BECs]) are the only two epithelial cell lineages among various types of the constituent cells. Cells that give rise to both hepatocytes and BECs are generally regarded as bipotential liver progenitors or stem cells. In liver development, hepatoblasts emerging from the foregut endoderm fulfill this criterion and are thus considered to be fetal liver stem/progenitor cells (Tanimizu and Miyajima 2007). During adult liver homeostasis, liver maintenance is achieved by cell division of mature hepatocytes and BECs (Ponder 1996). It is important to note that the adult liver can regenerate under conditions of massive parenchymal loss. After surgical removal or partial hepatectomy (PHx), residual mature hepatocytes restore the liver mass. The contribution of liver stem/progenitor cells to regeneration seems to be minimal if any in this type of liver injury (Michalopoulos and DeFrances 1997), although several recent studies have suggested the presence of newborn hepatocytes originating from sources other than pre-existing hepatocytes (Furuyama et al. 2011; Iverson et al. 2011; Malato et al. 2011). In contrast, when the liver is severely damaged, as in the case of hepatocyte-selective proliferation defect caused by some drugs or toxins, the contribution of adult liver progenitor cells (LPCs) is assumed (Fausto 2004; Knight et al. 2005; Bird et al. 2008; Duncan et al. 2009). The LPCs are a cell population with a high nuclear/cytoplasmic ratio and are known as "oval cells" in rodent models because of their ovoid appearance (Farber 1956). Upon liver damage, LPCs emerge from periportal regions, proliferate extensively, migrate into the hepatic lobule, and are considered to differentiate into both hepatocytes and BECs (Fausto 2004; Knight et al. 2005). As these types of progenitor cells are not observed in the uninjured liver, they are

[5]These two authors contributed equally to this work.
[6]Present address: Howard Hughes Medical Institute, Department of Developmental Biology, Stanford University, School of Medicine, Stanford, CA 94035, USA.
[7]Corresponding author
E-mail itohru@iam.u-tokyo.ac.jp
Article published online ahead of print. Article and publication date are online at http://www.genesdev.org/cgi/doi/10.1101/gad.204776.112.

often referred to as facultative stem/progenitor cells in the adult liver (Alison et al. 1996; Yanger and Stanger 2011).

There are several experimental models to induce LPCs. In mice, 3,5-diethoxycarbonyl-1,4-dihydrocollidine (DDC) diet and choline-deficient, ethionine-supplemented (CDE) diet models are often used (Preisegger et al. 1999; Akhurst et al. 2001). The LPC response, also termed as ductular reaction, has been found in human chronic liver diseases and severely injured livers, such as acute hepatitis, fulminant hepatitis, cholestatic disorders, and liver cancers (Libbrecht and Roskams 2002; Turanyi et al. 2010). This suggests that LPCs are broadly activated to restore the function of the liver when mature hepatocytes fail to proliferate. Despite previous notions that the degree of the LPC response correlates with the severity of liver disease (Lowes et al. 1999), it has not been demonstrated whether LPCs indeed engage in liver regeneration. In addition, the underlying mechanism of the activation of LPCs still remains largely unknown.

As liver injuries accompanying the LPC responses are usually associated with inflammation and fibrosis, interaction between LPCs and multiple other cell populations, such as immune cells and fibroblastic cells, has been postulated. In many cases of adult stem/progenitor cell regulation, the importance of the extracellular signals provided by the surrounding cells, forming the so-called stem cell niche, are well recognized. However, little has been documented as to whether and how the LPCs are regulated by the niche signals. Cell-to-cell interactions involve paracrine growth factors and cytokines that can be grouped into several major families (Gerhart 1999), among which the fibroblast growth factor (FGF) family is one of the best characterized. FGFs constitute a family of growth factors that have diverse activities in development and adulthood. It has been reported that FGF signals participate in tissue development and organization, branching morphogenesis, angiogenesis, and wound repair, as well as the regulation of stem cell systems in various organs (Itoh and Ornitz 2008; Turner and Grose 2010). The mammalian FGF family is classified as paracrine (canonical) ligands, endocrine ligands, and FGF homologous factors. The paracrine FGF families can be further subdivided into five subfamilies—FGF1/2, FGF3/7/10/22, FGF4/5/6, FGF8/17/18, and FGF9/16/20—in mice and humans. There are four members of the FGF receptor family: FGFR1, FGFR2, FGFR3, and FGFR4. Since FGFR1, FGFR2, and FGFR3 each have splice variant isoforms "b" and "c," seven different FGFR subtypes can be expressed. It is known that their specific functions are achieved by spatially and temporally regulated expression patterns of particular ligands and receptors; for example, the FGF3/7/10/22 subfamily ligands are typically expressed by mesenchymal cells and exert their effects through the cognate receptor FGF receptor 2 isoform IIIb (FGFR2b), whose expression is restricted in epithelial cells (Steiling and Werner 2003).

In the present study, we aimed at elucidating the cellular and molecular framework that underlies the LPC regulation upon liver injury. Based on the characteristic expression profile and the results of in vivo functional analyses, we found evidence that FGF7 is an essential signal for induction of the LPC response and contributes to the progenitor-dependent liver regeneration.

## Results

### *Thy1$^+$ cell population is a candidate for the LPC niche*

As previous studies have suggested that nonepithelial populations such as mesenchymal cells and immune cells reside near and around LPCs (Paku et al. 2001; Knight et al. 2007; Strick-Marchand et al. 2008), we suspected that those cells may functionally interact with LPCs and provide a putative LPC niche. To identify and characterize such an LPC–niche interaction, we first induced the LPC response in the mouse liver with a well-established protocol of the hepatotoxin DDC diet application (Preisegger et al. 1999). Cytokeratin 19$^+$ (CK19$^+$) LPCs expanded from around the portal vein after liver damage by feeding DDC diet (Fig. 1A). Immunostaining of the liver sections with several cell surface markers led to the finding that a Thy1$^+$ cell population appeared in close proximity to LPCs in DDC-induced liver damage (Fig. 1A). We selected and focused on this marker for further analysis, as its expression in injured livers has also been described in rats and humans (Dezso et al. 2007; Yovchev et al. 2009). An established marker for fibroblastic cells (Elastin) and a stellate cell marker (Desmin) partially overlapped with the Thy1$^+$ area (Supplemental Fig. S1A,B). Quantitative analysis of the Thy1 and CK19 immunostaining revealed that the expansion of Thy1$^+$ cells occurred prior to LPC activation (Fig. 1B). Thus, we presumed that Thy1$^+$ cells could provide a niche for LPCs that allows them to proliferate.

We sought to identify the nature of the niche signals for LPCs possibly provided by Thy1$^+$ cells. Among several major groups of paracrine factors, we especially focused on the FGF family because an LPC-specific marker, Trop2 (Okabe et al. 2009), has previously been reported as a target gene of FGF10 in lung development (Lu et al. 2005). We analyzed expression patterns of all of the paracrine *Fgf* ligands and found *Fgf7* to be highly expressed, while we could not detect any expression of *Fgf10* or *Fgf3/22* belonging to the same subfamily (Supplemental Fig. S2). The expression of *Fgf7* was increased significantly during the time course of DDC-induced liver damage, along with that of *Epcam* and *Krt19*, encoding the LPC/BEC markers epithelial cell adhesion molecule (EpCAM) and CK19, respectively (Fig. 1C). Accordingly, expression of FGF7 protein was barely detected in normal livers but was markedly induced in the vicinity of LPCs after DDC (Fig. 1D,F). Intriguingly, some Thy1$^+$ cells costained with FGF7 in the injured liver (Fig. 1E). We also examined a recovery model for liver injury, where mice were initially fed a DDC diet for 4 wk and then returned to the normal diet for another 2 wk (Supplemental Fig. S3). In this injury/recovery setting, the overall level of *Fgf7* expression strongly correlated with that of the LPC response as well as the progression of liver damage as measured by serum markers. These results suggest that FGF7 is a strong candidate for the niche signal for LPCs.

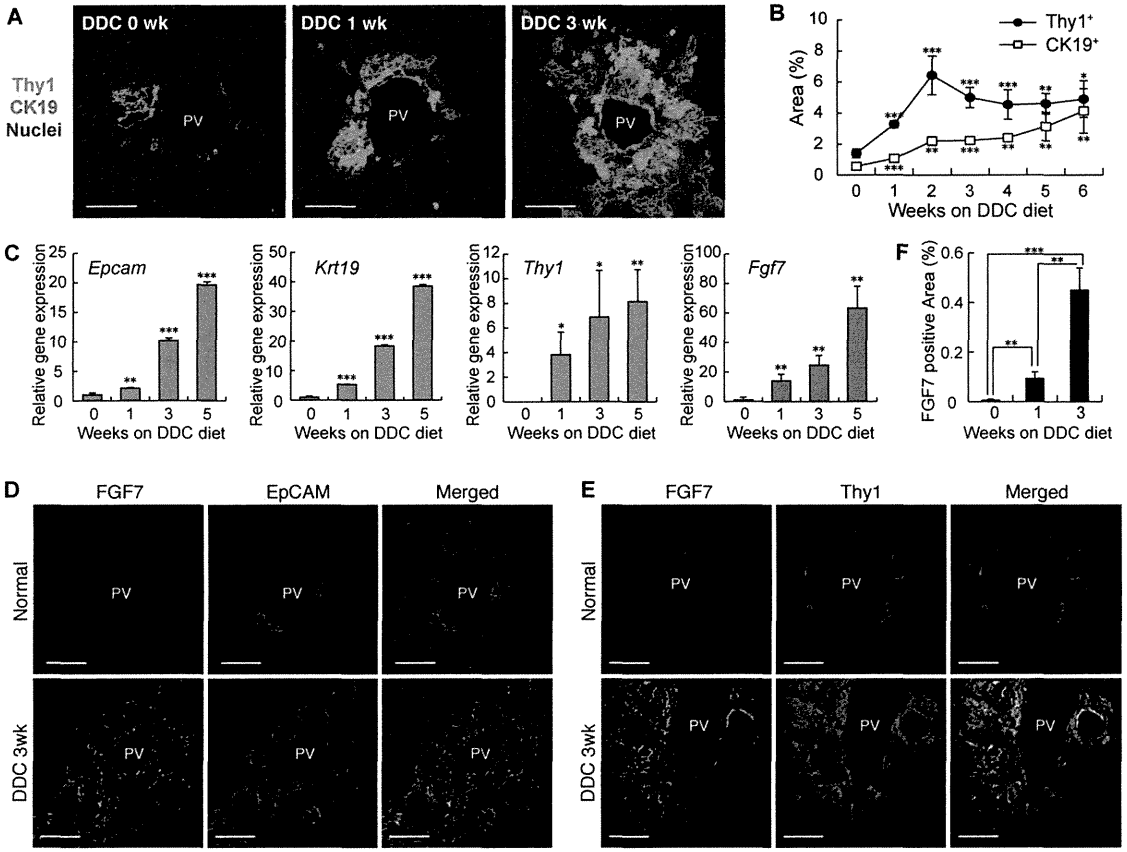


**Figure 1.** FGF7 expression in the damaged liver is up-regulated around LPCs. (*A*) Liver sections prepared from DDC diet-fed mice were subjected to immunofluorescent double-staining analysis. Thy1$^+$ cells (green) were observed in the immediate vicinity of CK19$^+$ LPCs (red) during the course of LPC activation. Bars, 80 μm. (PV) Portal vein. (*B*) Thy1- and CK19-positive areas were increased in the DDC-treated livers, as determined by quantitative analysis of immunofluorescence-stained images. Mean ± SD ($n = 3$). (***) $P < 0.001$; (**) $P < 0.01$; (*) $P < 0.05$, compared with normal liver (0 wk). (*C*) Total RNA was isolated from whole-liver samples of normal diet-fed (0 wk) or DDC diet-fed mice, reverse-transcribed, and subjected to quantitative PCR analyses to determine expression of the LPC markers *Epcam* and *Krt19*, the mesenchymal cell marker *Thy1*, and *Fgf7*. Expression was normalized to that of *Gapdh*. Mean ± SD ($n = 3$). (***) $P < 0.001$; (**) $P < 0.01$; (*) $P < 0.05$, compared with the value at 0 wk. (*D,E*) Confocal immunofluorescence images of the livers show that FGF7 (green) protein localized in the proximity of EpCAM$^+$ LPCs (*D*, red) and colocalized with Thy1$^+$ mesenchymal cells (*E*, red) in the periportal region in injured livers. Bars, 50 μm. (PV) Portal vein. (*F*) Expression of FGF7 protein was increased in the DDC-treated livers, as determined by quantitative analysis of immunofluorescence-stained images of at least 11 periportal fields from three livers for each time point. Mean ± SE. (***) $P < 0.001$; (**) $P < 0.01$.

### *LPCs receive the FGF7 signal from Thy1$^+$ mesenchymal cells*

To determine whether FGF7 can act on LPCs directly, we analyzed the expression of the FGF7 receptor FGFR2b in LPCs. In situ hybridization analysis of liver sections detected expression of the *Fgfr2* transcript in the CK19$^+$ LPC population (Fig. 2A). To validate expression of the cognate isoform for FGF7, EpCAM$^+$ LPCs and EpCAM$^-$ cells were isolated from the nonparenchymal cell (NPC) population of the DDC-treated liver and immunostained with a IIIb isoform-specific anti-FGFR2 antibody. We detected strong expression of FGFR2b in EpCAM$^+$ cells but not in EpCAM$^-$ cells (Fig. 2B,C).

We next performed quantitative PCR analysis using specific cell populations to further confirm the FGF7-producing cells and their target cells. Hepatocyte, NPC, EpCAM$^+$ LPC, Thy1$^+$ CD45$^-$ cell (Thy1$^+$ MC [for mesenchymal cell]) (see below), Thy1$^+$ CD45$^+$ cell (T-cell), and Thy1$^-$ CD45$^+$ cell (blood cell) fractions were isolated from the livers of mice fed DDC. We checked for adequate cell separation by the specific expression of each marker (Supplemental Fig. S3A). As expected from the aforementioned immunostaining patterns, *Fgf7* and *Fgfr2* isoform IIIb were detected in Thy1$^+$ MC and LPC fractions, respectively (Fig. 2D). These results suggest that FGF7 signal may function directionally from Thy1$^+$ CD45$^-$ cells to LPCs. The Thy1$^+$ CD45$^-$ cells strongly expressed *Elastin* (*Eln*), *nerve growth factor receptor* (*Ngfr*; p75NTR) and *α smooth muscle actin* (*Acta2*; α-SMA), which are markers for fibroblastic cells, hepatic stellate cells, and myofibroblasts, respectively (Fig. 2D; Supplemental Fig. S4A). Thus, they are considered to be a mesenchymal cell population and distinct from T-cell populations. We also

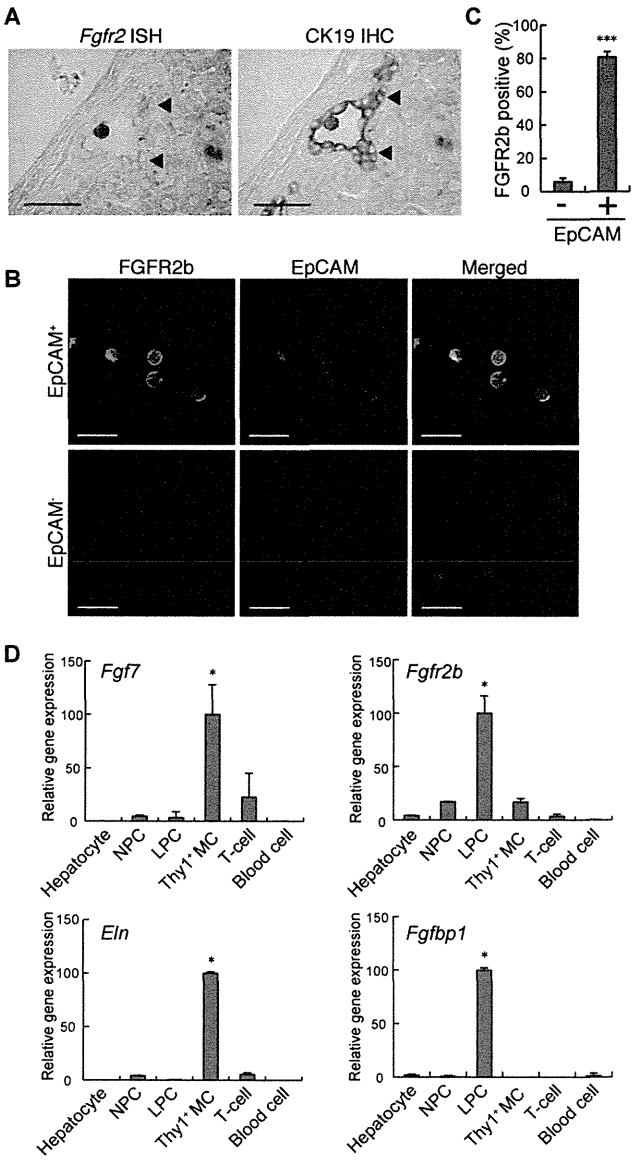


**Figure 2.** FGF7 signal emanates from Thy1$^+$ cells and acts on LPCs. (*A*, *left* panel) Liver sections prepared from mice fed DDC diet for 3 wk were subjected to in situ hybridization analysis for *Fgfr2* expression. (*Right* panel) The same section was subsequently overlaid with immunohistochemical staining using anti-CK19 antibody to confirm its expression in LPCs. Bars, 200 μm. (*B*,*C*) EpCAM$^+$ and EpCAM$^-$ cells were sorted from NPCs in the livers of the mice fed the DDC-containing diet for 5 wk. Cytospin preparations of these cells were stained for FGFR2b (green) and EpCAM (red). Representative images are shown in *B*, and the result of quantitation are shown in *C* (EpCAM$^-$, $n$ = 980; EpCAM$^+$, $n$ = 1454). Mean ± SD. Bars, 40 μm. (***) $P < 0.001$. (*D*) Hepatocyte, NPC, EpCAM$^+$ cell (LPC), Thy1$^+$ CD45$^-$ mesenchymal cell (Thy1$^+$MC), Thy1$^+$ CD45$^+$ T-cell (T-cell), and Thy1$^-$ CD45$^+$ cell (blood cell, excluding T-cell) fractions were isolated from the livers of DDC-treated mice. Expression of the indicated genes was examined by quantitative RT–PCR. Mean ± SD ($n$ = 3). (*) Significantly different from each of the other five fractions (ANOVA, with Tukey post hoc tests, $P < 0.05$).

performed genetic lineage tracing experiments using an *Alfp-Cre* transgenic (Tg) mouse strain, where expression of the Cre recombinase occurred in fetal hepatoblasts and adult hepatocytes and hence enabled us to label and track their descendants. After DDC injury, hepatocytes, BECs, and LPCs were virtually all lineage-labeled. Thy1$^+$ cells, on the other hand, were of a distinct lineage from liver epithelial cells (Supplemental Fig. S4B,C).

FGF-binding protein 1 (FGFBP1) is a soluble protein that can bind a subset of FGFs, including FGF7, and enhance their activities (Beer et al. 2005). Previous studies on skin and renal tube regeneration have shown FGFBP1 to be expressed in epithelial cells rather than mesenchymal cells and to be a target of FGF7 signaling (Liu et al. 2001; Beer et al. 2005). *Fgfbp1* was almost exclusively expressed in LPCs, which further strengthened the notion that LPCs are the primary target of FGF7 signaling from Thy1$^+$ cells (Fig. 2D).

### *Up-regulation of FGF7 is concurrent with expansion of LPCs and Thy1$^+$ cells*

We then examined the correlation of FGF7 with the induction of LPCs and Thy1$^+$ cells in other models of liver injury. First, ligation of the common bile duct (BDL) in mice was used as a model for cholestatic liver disease. FGF7 expression was increased in the BDL-manipulated liver with the LPC response (Fig. 3A,B). As is the case with DDC-induced liver injury, FGF7 in this model was also produced predominantly in Thy1$^+$ cells, while LPCs were the primary target for the signal by expressing the receptor (Supplemental Fig. S5). Second, we checked the activation of LPCs and expression of FGF7 in liver-specific *Tak1*-deficient (*Alfp-Cre*; *Tak1$^{flox/flox}$*, hereafter referred to as *Tak1*-LKO) mice. Loss of *Tak1* in the liver results in chronic inflammation and eventually leads to fibrosis and carcinogenesis (Bettermann et al. 2010; Inokuchi et al. 2010). It is thus considered a faithful model for the progression of human liver diseases. We observed apparent LPC response and expansion of Thy1$^+$ cells in 8-wk-old *Tak1*-LKO mice (Fig. 3C). Concomitantly with the increase of CK19-positive (Fig. 3E) and Thy1-positive (Fig. 3F) areas, the expression of FGF7 was significantly induced (Fig. 3D,G). Although the immunostaining results showed some colocalization of FGF7 with EpCAM$^+$ LPCs, gene expression analysis using isolated cell fractions confirmed that, also in this model, *Fgf7* was mainly produced in Thy1$^+$ cells but not in LPCs (Supplemental Fig. S6). Finally, serum FGF7 levels were found to be increased in human patients with liver diseases such as fulminant hepatic failure and acute hepatitis (Fig. 3H), which often accompany LPC activation. Together, these data suggest that induction of FGF7 upon liver disorders associated with the LPC response is generally conserved in both rodents and humans.

### *FGF7 plays a necessary function as a niche signal for induction of LPCs*

To address the physiological relevance of FGF7 expression in the course of the LPC response, we used *Fgf7*

knockout mice (Guo et al. 1996). They exhibit relatively normal growth and are fertile, with some phenotypes including defects in kidney development, postnatal thymic regeneration, and neurogenesis in the hippocampus (Qiao et al. 1999; Alpdogan et al. 2006; Terauchi et al. 2010; Lee et al. 2012). No liver phenotype during development or in adulthood has been reported. In order to analyze the LPC response in *Fgf7* knockout mice, adult littermates of wild-type and knockout mice were fed a DDC-containing diet or subjected to BDL. We measured the degree of LPC activation by CK19 immunostaining and confirmed that CK19$^+$ LPC numbers were increased by DDC or BDL in the wild-type liver (Fig. 4A,H).

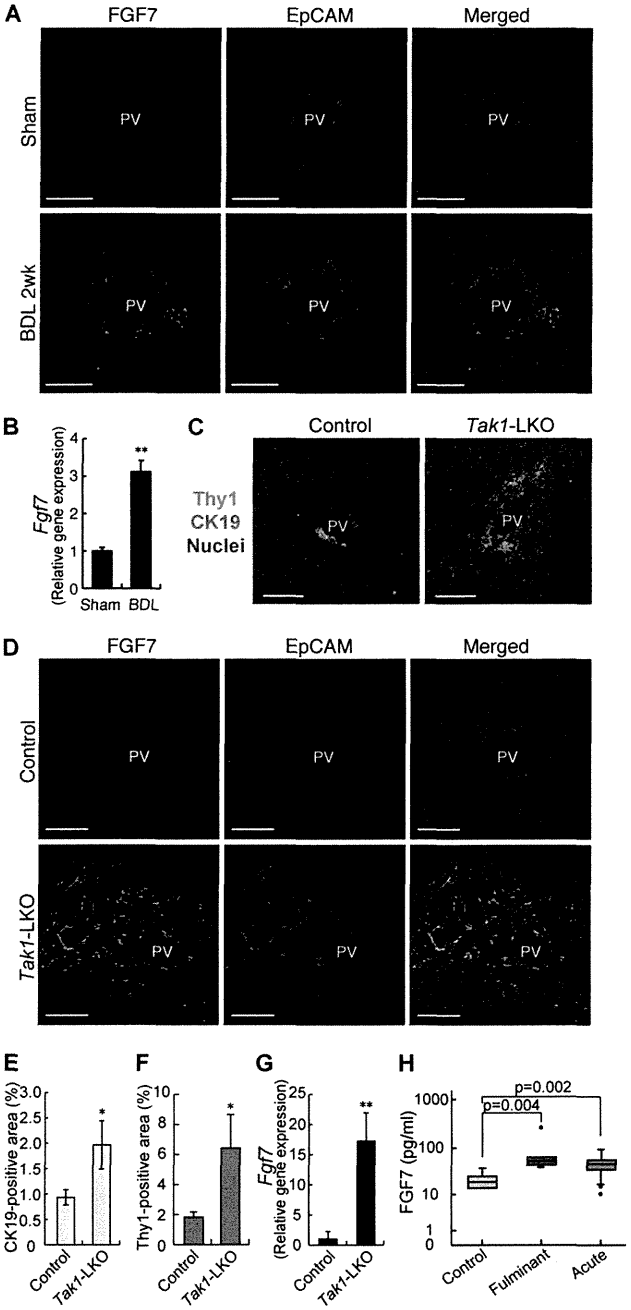


However, the LPC response was almost completely suppressed in *Fgf7* knockout mice (Fig. 4A,B,H,I). In contrast, quantitative analysis of the Thy1$^+$ area in *Fgf7* knockout mice revealed little change when compared with the wild-type control in both normal and damaged livers (Fig. 4C,J). In other words, Thy1$^+$ cells were capable of expanding in response to liver damage even in the absence of FGF7 function, consistent with the notion that FGF7 acts directly on LPCs rather than upstream of Thy1$^+$ cells. Ki67 or TUNEL staining with CK19 revealed that Ki67$^+$ proliferating cells among the CK19$^+$ LPCs were significantly decreased, although not completely abrogated, in the knockout mice compared with the wild-type control, while no statistically significant difference was observed in the TUNEL$^+$ cell population (Supplemental Fig. S7). These results suggest that the suppressed LPC response in *Fgf7* knockout mice can be attributed, at least in part, to reduced proliferation of LPCs rather than augmented induction of their apoptosis.

*Fgf7* knockout mice were highly sensitive to DDC and had a low survival rate, whereas the wild-type mice were more resistant to hepatotoxin-induced liver injury (Fig. 4D). Upon DDC administration, systemic symptoms were obvious and generally more severe in the knockout than in the wild-type control, including jaundice, hemorrhagic diathesis, and weight loss, which are typically observed in end-stage liver disease (Figs. 4E,F; data not shown). Gross pathological and histopathological examinations of the mice that survived at 11 wk of injury confirmed that liver failure with severe leakage of bile into the liver vasculature is the most plausible cause of death in *Fgf7* knockout mice, while no fatal abnormality was recognized in any organs/tissues other than the liver (data not shown). We also performed serum biochemical tests using the mice fed DDC for 10 wk. The cholestasis markers total bilirubin (TBIL) and alkaline phosphatase (ALP) were both

**Figure 3.** FGF7-mediated LPC activation is conserved in several liver injuries. (*A,B*) Liver samples prepared from sham-operated (Sham) or BDL mice were subjected to the following experiments. (*A*) Confocal immunofluorescent double staining using anti-FGF7 (green) and anti-EpCAM (red) antibodies. Bars, 50 μm. (PV) Portal vein. (*B*) Quantitative RT–PCR analysis of *Fgf7* mRNA. Mean ± SE ($n$ = 3). (**) $P < 0.01$. (*C–G*) Liver samples from 8-wk-old liver-specific *Tak1*-LKO (*Alfp-Cre; Tak1$^{flox/flox}$*) or control (*Tak1$^{flox/flox}$*) mice were subjected to the following experiments. (*C*) Representative images for immunofluorescent double staining of CK19 (red) and Thy1 (green). (PV) Portal vein. Bars, 80 μm. (*D*) Confocal immunofluorescent double staining using anti-FGF7 (green) and anti-EpCAM (red) antibodies. Bars, 50 μm. (PV) Portal vein. (*E*) Quantitative image analysis of CK19-positive area. Mean ± SD ($n$ = 3). (*) $P < 0.05$. (*F*) Quantitative image analysis of Thy1-positive area. Mean ± SD ($n$ = 3). (*) $P < 0.05$. (*G*) Quantitative RT–PCR analysis of *Fgf7* mRNA. Mean ± SD ($n$ = 3). (**) $P < 0.01$. (*H*) Serum FGF7 levels in human samples. enzyme-linked immunosorbent assay (ELISA) for human FGF7 was performed on serum samples harvested from healthy controls ($n$ = 6) and patients with fulminant ($n$ = 6) or acute ($n$ = 43) hepatitis. The data are presented as median (25–75 percentile).

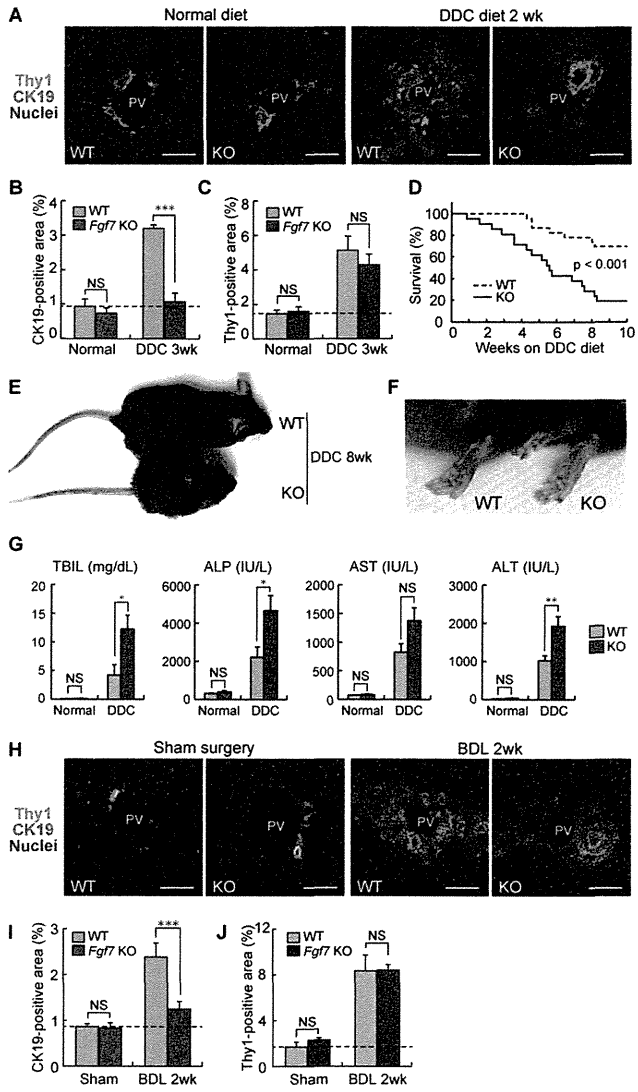


**Figure 4.** FGF7 is essential for LPC activation and liver regeneration in injured livers. Adult littermates of *Fgf7* knockout (KO) and wild-type (WT) mice were fed normal or DDC diet (*A–G*) or subjected to BDL or a sham operation (*H–J*). (*A,H*) Representative images for immunofluorescent double staining of CK19 (red) and Thy1 (green). Bars, 80 μm. (PV) Portal vein. (*B,I*) Quantitative image analysis of CK19-positive area. Mean ± SD ($n = 3$). (***) $P < 0.001$; (NS) not significant. (*C,J*) Quantitative image analysis of Thy1-positive area. Mean ± SD ($n = 3$). (NS) Not significant. (*D*) Kaplan-Meier survival curves of control (wild-type, $n = 23$) and *Fgf7* knockout ($n = 21$) mice given DDC, showing that the lack of FGF7 leads to the increased mortality after DDC feeding. Statistical analysis was performed using the log-rank (Mantel-Cox) test. (*E,F*) Appearance of *Fgf7* knockout and wild-type mice fed DDC diet for 8 wk. (*F*) More severe symptoms for jaundice, such as yellow-colored skin, were typically observed in the knockout animal. (*G*) Serum TBIL, ALP, AST, and ALT levels were measured in control and *Fgf7* knockout mice fed a normal (wild type, $n = 3$; knockout, $n = 3$) or DDC-containing (wild type, $n = 6$; knockout, $n = 3$) diet for 10 wk. Mean ± SE. (**) $P < 0.01$; (*) $P < 0.05$; (NS) not significant.

significantly increased in *Fgf7* knockout mice (Fig. 4G). At the same time, the level of the hepatocyte injury marker alanine transaminase (ALT) was significantly elevated in the knockout mice compared with the wild type, and that of aspartate transaminase (AST) also trended higher, but the difference was not statistically significant (Fig. 4G). At that point, the LPC numbers in the knockout mice could not keep up with those in wild-type mice (Supplemental Fig. S8A–C). These results indicate that the lack of FGF7 exacerbates damages in both hepatocytes and bile ducts and that the LPC response directly correlates with liver function and survival of an organism upon toxic insult. Taken together, we conclude that FGF7 is necessary for LPC activation in vivo at least in two different experimental models, and its expression and function may counter liver dysfunction.

### *Forced expression of FGF7 is sufficient to induce expansion of the LPC population in vivo*

We next performed gain-of-function experiments to further explore the function of FGF7 in regulating the LPC response. First, we examined the effect of FGF7 on LPCs in vitro. We found that a recombinant FGF7 stimulated the proliferation of HSCE1, a cell line derived from EpCAM$^+$ LPCs of adult mice (Okabe et al. 2009), in a dose-dependent manner (Fig. 5A). To examine the effect of FGF7 in vivo, we used *Alfp-Cre; Rosa26-rtTA-IRES-EGFP; tetO-CMV-FGF7* triple Tg mice in which overexpression of FGF7 in the liver is achieved by doxycycline (Dox) treatment (Fig. 5B,C). A significant increase in CK19$^+$ LPC-like cell numbers was observed in the periportal regions of the triple Tg (hereafter referred to as *FGF7* Tg) mouse livers compared with control *Alfp-Cre; Rosa26-rtTA-IRES-EGFP* double Tg mouse livers (Figs. 5D,E). These expanding cells coexpressed other well-known LPC markers: A6, EpCAM, and SOX9 (Fig. 5E; Supplemental Fig. S9A,B). Notably, A6$^+$ CK19$^-$ cells, which can be regarded as a fraction of newly formed hepatocytes (Engelhardt et al. 1990; Ishikawa et al. 2012), were clearly detected adjacent to A6$^+$ CK19$^+$ LPCs in *FGF7* Tg mouse livers as well as in DDC-injured livers (Fig. 5D; Supplemental Fig. S6A), implying that the cell population induced by FGF7 has a potential to differentiate to hepatocytes.

Previous studies have shown that the extracellular matrix (ECM) plays an important role in regulating the LPC response and liver regeneration (Boulter et al. 2012; Español-Suñer et al. 2012). Immunostaining analysis of the type I and type III collagen proteins revealed that there was a significant accumulation of these ECM components around the expanding LPCs in response to FGF7 overexpression, similar to the case observed in the livers of DDC-treated animals (Fig. 5G). This strongly supports the notion that the FGF7-induced LPC induction in the normal liver faithfully recapitulates the phenomenon that occurs under the pathophysiological conditions in diseased livers. Meanwhile, the level of collagen gene expression (*Col1a1* and *Col3a1* for type I and type III collagens, respectively) using the whole-liver mRNA samples showed no significant increase in the expression of

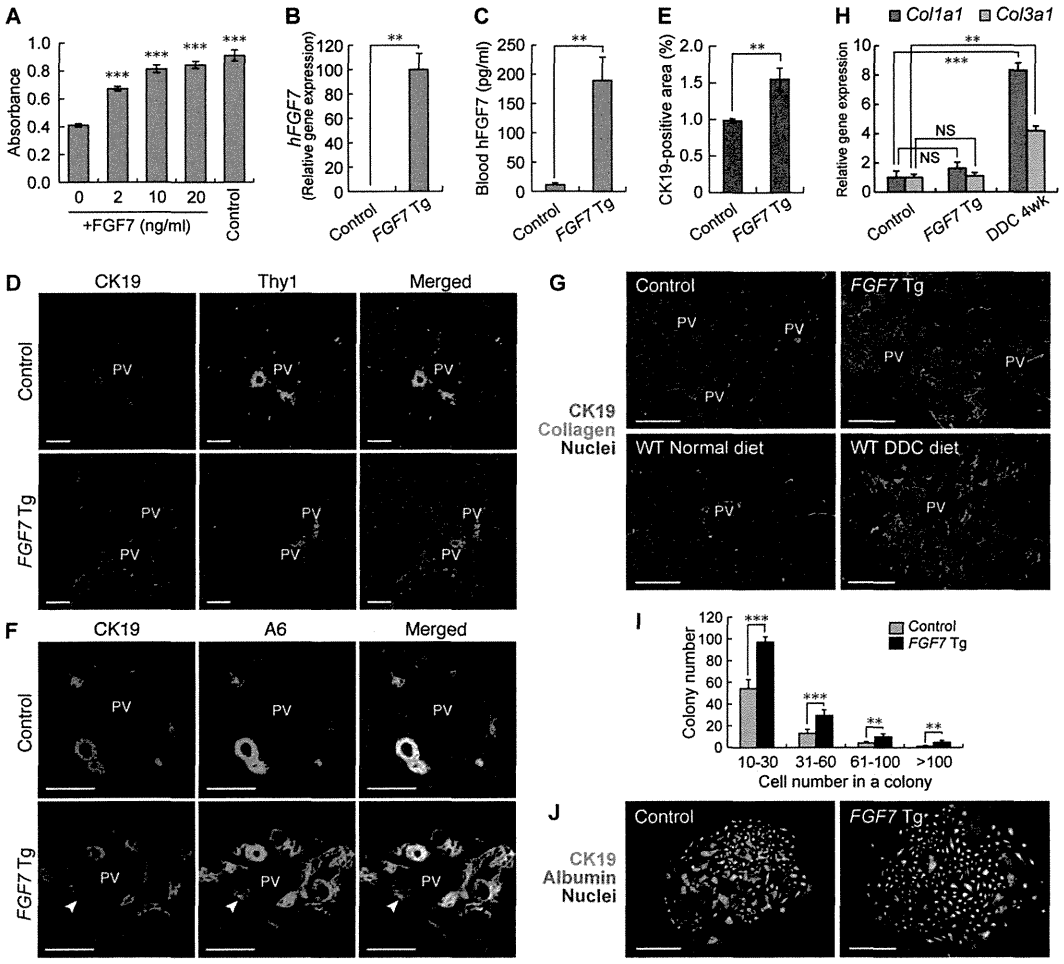


**Figure 5.** Overexpression of FGF7 can induce the LPC response in the adult mouse liver. (*A*) The level of proliferation of HSCE1 cells was examined by WST-1 assay. Stimulation with epidermal growth factor (EGF) and hepatocyte growth factor (HGF) was used as a control. Mean ± SD ($n$ = 3). (***) $P < 0.001$ compared with no cytokine treatment (0). (*B*) Quantitative RT–PCR analysis was performed to assess human *FGF7* mRNA levels in the liver after 3 wk of Dox administration. Mean ± SE (control, $n$ = 3; Tg, $n$ = 5). (**) $P < 0.01$. (*C*) Serum levels of human FGF7 protein after 3 wk of Dox administration were determined by ELISA. Mean ± SE (control, $n$ = 4; Tg, $n$ = 6). (**) $P < 0.01$. (*D*) Immunostaining of CK19 (red) and Thy1 (green) in the livers of *FGF7* Tg mice and control mice treated with Dox for 4 wk. Bars, 100 μm. (PV) Portal vein. (*E*) Quantitative analysis of CK19-positive areas showed an increased number of LPC-like cells in *FGF7* Tg mice treated with Dox for 4 wk. Mean ± SD ($n$ = 3). (**) $P < 0.01$. (*F*) Immunostaining of CK19 (red) and A6 (green) showed expansion of CK19$^+$ A6$^+$ LPCs in the livers of *FGF7* Tg mice treated with Dox for 4 wk. CK19$^-$ A6$^+$ newly formed hepatocytes were also observed (arrowheads). Bars, 50 μm. (PV) Portal vein. (*G*) Immunostaining of CK19 (red) and collagen (green) in the livers of *FGF7* Tg and control mice, wild-type mice fed a normal diet, and DDC-treated wild-type mice. Bars, 100 μm. (PV) Portal vein. (*H*) Quantitative RT–PCR analysis of *Col1a1* and *Col3a1* mRNA. Mean ± SE (control, $n$ = 3; Tg, $n$ = 5; DDC, $n$ = 3). (**) $P < 0.01$; (***) $P < 0.001$; (NS) not significant. (*I*) EpCAM$^+$ cells were isolated from the livers of *FGF7* Tg mice and control mice 3 wk after Dox treatment and subjected to the in vitro colony formation assay. Mean ± SD ($n$ = 3). (**) $P < 0.01$; (***) $P < 0.001$. (*J*) Immunofluorescence images of representative large colonies stained with anti-CK19 (green) and albumin (red). Bars, 200 μm.

either of these genes at the whole-organ level (Fig. 5H). Thus, overexpression of FGF7 in the liver results in local deposition of ECMs associated with the LPC expansion but does not lead to a global fibrogenic response in the organ.

To further characterize the FGF7-induced LPC-like population in terms of functional criteria, we next performed clonogenic assays to evaluate its proliferative and bilineage differentiation potentials in vitro. It has been well documented that stem/progenitor cell activity of a certain population of liver cells can be defined by their capacity to generate large colonies that are capable of expressing both hepatocyte and BEC lineage markers in culture (Suzuki et al. 2008; Okabe et al. 2009; Dorrell et al. 2011; Shin et al. 2011). When EpCAM$^+$ cells isolated from the *FGF7* Tg mice and the control mice were subjected to in vitro colony formation assays (Okabe et al. 2009), the EpCAM$^+$ cells from the Tg mice formed colonies, including those composed of >100 cells (Fig. 5I). Immunostaining analyses confirmed that these large colonies were composed of both albumin-positive (the hepatocyte marker) and CK19-positive (the LPC/BEC marker)